communications biology

A Nature Portfolio journal

Article

https://doi.org/10.1038/s42003-026-09585-z

Sex- and etiology-specific effects on predictive processing in the inferior colliculus of two rat models of autism

Sara Cacciato-Salcedo [1,2,3], Ana B. Lao-Rodríguez[1,2,3] & Manuel S. Malmierca [1,2,3]

Atypical sensory processing is a common feature of autism, yet the neural computations that give rise to these differences, particularly in relation to biological sex and etiological origin, remain unclear. Here we examine predictive auditory processing at the single-neuron level in the inferior colliculus of two adult rat models of autism: a genetic model with a heterozygous *Grin2b* deletion (*Grin2b* + /–) and an environmental model based on prenatal valproic acid exposure. We recorded neuronal responses to an auditory oddball paradigm and a cascade control sequence across lemniscal and non-lemniscal IC divisions under high-intensity stimulation, allowing us to derive indices of repetition suppression, prediction error and neuronal mismatch. Using generalized linear mixed-effects models that accounted for animal identity, inferior colliculus division, sex, and rat model, followed by hierarchical group-level comparisons, we identified robust alterations in predictive processing in both autism-like models. These effects varied across inferior colliculus divisions and differed between sexes, revealing distinct phenotype-specific signatures. The results indicate that sex and etiology jointly modulate early auditory computations in autism. More broadly, our findings highlight the translational value of predictive coding frameworks and support the use of complementary animal models to capture neurobiological heterogeneity across the autism spectrum.

Autism spectrum disorder is a neurodevelopmental condition characterized by atypical social communication, restricted interests, and repetitive behaviors[1]. Among its most pervasive features is altered sensory processing, particularly in the auditory domain[2–4]. Approximately 90% of autistic individuals exhibit either heightened or diminished sensitivity to certain sounds, often modulated by contextual factors[5–7]. Divergences in the processing of auditory context may disrupt the integration of sensory cues with environmental demands, thereby exerting cascading effects on language acquisition, learning trajectories, and behavioral regulation throughout the lifespan[6,8–10].

Autism encompasses a heterogeneous array of developmental trajectories, influenced by both genetic and environmental factors. Rare, high-risk mutations in synaptic genes such as *Grin2b*, which encodes the GluN2B subunit of the N-methyl-D-aspartate (NMDA) receptor, have been implicated in monogenic forms of autism[11–13]. In addition, environmental insults during critical periods of neurodevelopment, such as prenatal exposure to valproic acid (VPA), an antiepileptic and mood-stabilizing drug, can increase the incidence of autism-like phenotypes by up to tenfold in offspring[14–16]. Increasing evidence suggests that genetic and environmental factors often interact, compounding risk and contributing jointly to the emergence of autism signs[17]. Further, biological sex modulates susceptibility to both pathogenic factors. Females tend to exhibit greater resilience, potentially via protective mechanisms involving heritable modifiers and phenotypic buffering, including the influence of sex chromosomes and fetal hormonal environments[18–20].

Indeed, autism is diagnosed more frequently in males, with an estimated male-to-female ratio of roughly 3:1[21]. However, accumulating evidence indicates that autistic traits might manifest differently in females[22–24]. Compared to males, autistic females tend to show fewer overt repetitive behaviors and engage more effectively in compensatory strategies during social interactions, which likely contributes to diagnostic underrecognition[24]. These phenotypic differences may reflect underlying sex-specific neurobiological mechanisms that are differentially engaged depending on context, although this possibility remains insufficiently examined.

The predictive coding theory offers a mechanistic framework for understanding context-dependent perception in both typical and atypical

[1]Cognitive and Auditory Neuroscience Laboratory, Institute of Neuroscience of Castilla y León (INCYL), Salamanca, Spain. [2]Salamanca Institute for Biomedical Research (IBSAL), Salamanca, Spain. [3]Department of Cell Biology and Pathology, Faculty of Medicine, University of Salamanca, Salamanca, Spain.
e-mail: msm@usal.es

neurodevelopment, including autism[25–30]. In this framework, the brain continuously generates predictions based on environmental regularities and compares them with incoming sensory input[25]. Discrepancies, termed prediction errors, update internal models to optimize future perception. This inferential architecture supports the suppression of redundant input and the enhancement of salient, unexpected events. In autism, predictive coding mechanisms may be divergent, resulting in heightened or blunted sensitivity to change and an unusual capacity to adapt to contextual demands[26,28,29]. Biological sex may further modulate predictive processes, though its role has yet to be systematically characterized.

At the single-neuron level, predictive processing can be quantified using three indices: repetition suppression (iRS), reflecting reduced responses to repeated stimuli; prediction error (iPE), indexing neural responses to deviant or unexpected events; and the neuronal mismatch index (iMM), which captures the net deviation from predicted input[31,32]. These neural phenomena have been widely used to study predictive dynamics in both neurotypical and clinical populations using electro and magnetoencephalography[33–42]. However, findings in autistic individuals remain inconsistent, with reports of both exaggerated and attenuated mismatch responses[38,42]. These discrepancies may arise from methodological variability, differences in stimulus design, or insufficient modeling of key moderators such as sex and etiological origin. Recent findings suggest that females with autism may exhibit intermediate or even enhanced predictive responses compared to male counterparts and neurotypical females[36], further underscoring the need for sex-specific analyses. Hence, it is essential to characterize both male and female phenotypes and to determine how biological sex and etiology modulate the neuronal mechanisms underlying contextual processing in autism.

Here, we investigated how biological sex and etiology (hereafter, *rat model*) influence predictive auditory processing at the single-neuron level in two rat models of autism at adult stages. Using *Grin2b* heterozygous mutants (*Grin2b* + /–) and prenatally VPA-exposed rats, we recorded single-unit activity across the two main auditory pathways within the inferior colliculus (IC): the lemniscal IC, which primarily encodes stimulus-driven acoustic features, and the non-lemniscal IC, which integrates contextual information[43–45]. Consequently, the IC functions as a midbrain hub where ascending auditory inputs converge with descending cortical signals[46–50] to encode auditory context[32,51–56].

We presented oddball and cascade control sequences under high-intensity stimulation to elicit deviant, cascade, and standard responses, allowing us to quantify iRS, iPE, and iMM. In the oddball paradigm, a rare deviant tone was interspersed among frequent standard tones to evoke context-dependent mismatch responses[57]. The cascade paradigm consisted of a predictable series of tones arranged in ascending or descending order without immediate repetitions, controlling for adaptation effects while preserving stimulus predictability[57,58].

To examine the effects of sex, rat model, and IC division, we fitted generalized linear mixed-effects models to each elicited response and baseline neural activity, and performed group-level contrast estimate comparisons. This hierarchical approach revealed distinct contributions of sex and rat model to context-dependent auditory processing within the IC, providing mechanistic insight into early predictive computations in autism-like perception.

Results

We recorded single-unit activity from the lemniscal and non-lemniscal divisions of the IC in control rats and in two autism-like models, *Grin2b* +/– and prenatal VPA-exposed offspring (Figs. 1–3). Before evaluating tone-evoked responses, we quantified pre-stimulus baseline activity for each neuron to establish IC division- and group-specific firing characteristics in the absence of auditory input. Then, we derived spike-density functions for deviant (DEV), cascade (CAS), and standard (STD) tones across all groups (Fig. 4, Supplementary Data 1), and obtained the corresponding baseline-corrected spike counts to characterize auditory processing under these contextual conditions. From these responses, we extracted the predictive components of mismatch processing by computing DEV–STD for iMM, CAS–STD for iRS, and DEV–CAS for iPE.

To determine how baseline and context-dependent neural activity, and the resulting predictive computations, differed by sex, etiological origin, and IC division, we aggregated neural activity at the subject × division level so that each animal contributed a single, biologically meaningful estimate to group-level comparisons.

Then, we fitted generalized mixed-effects models to baseline activity, evoked neuronal responses, and the three predictive components of mismatch processing (iMM, iRS, iPE), specifying random intercepts for subjects and random slopes for IC division to preserve the hierarchical structure of the data. To quantify sex- and model-specific effects within each IC division, we extracted post hoc contrast estimates from the fitted models and conducted the corresponding pairwise comparisons (Figs. 5–7, Supplementary Data 2-4).

Finally, to relate context-dependent adaptation dynamics to mismatch processing, we briefly assessed whether the rate of short-term adaptation decay, captured by the *b* coefficient from a power-law fit to the first ten STD trials, correlated with the repetition suppression phenomenon across rat groups (Fig. 8, Supplementary Data 5). Subsequent sections present these analyses and their implications for predictive coding in the inferior colliculus.

Pre-stimulus baseline activity

First, we quantified pre-stimulus baseline activity as the spontaneous firing rate during the 75 ms window immediately preceding auditory onset. This measure indicated the tonic excitability and contextual state of IC neurons before sensory input.

We fitted generalized linear mixed-effects models with fixed effects for IC division (lemniscal and non-lemniscal), sex (female, male), and rat model (Control, *Grin2b* + /–, VPA), including all interaction terms. To capture within-subject variability across divisions, we specified random intercepts for animals and random slopes for IC division. The model included 68 division-level observations for 46 animals.

The model showed excellent fit, with an intraclass correlation coefficient of 0.899, and demonstrated strong predictive accuracy, yielding a cross-fold median absolute error of 0.339 spikes/s. These indices indicated that between-animal factors accounted for most of the variability in pre-stimulus baseline activity.

The model revealed significant main effects of IC division ($p = 0.002$), sex ($p = 0.002$), and prenatal VPA administration ($p = 0.020$). It also identified significant Division x Sex ($p = 0.020$), and Sex x VPA ($p = 0.048$) interactions (Supplementary Information, Table 1), indicating that the influence of sex on pre-stimulus baseline activity differed across IC divisions and mainly depended on prenatal VPA-induced perturbations.

Post hoc contrasts further clarified the patterns revealed by the mixed models (Supplementary Information, Table 2). In the lemniscal IC, control females showed higher pre-stimulus baseline activity than control males (contrast estimate = 5.678, $p = 0.001$; Fig. 5A). Among females, prenatal VPA exposure significantly reduced baseline activity relative to controls (contrast estimate = 4.862, $p = 0.017$; Fig. 5A). In males, none of the autism-like conditions produced significant differences. In the non-lemniscal IC, the above patterns persisted. Control females again exceeded males (contrast estimate = 9.221, $p = 0.014$; Fig. 5B), confirming a robust female-biased baseline regime. The VPA-induced females exhibited lower pre-stimulus baseline activity than controls (contrast estimate = 1.181, $p = 0.040$; Fig. 5), whereas no significant contrasts emerged among males.

Collectively, these results show that female-biased tonic excitability was most prominent under control conditions and was selectively reduced by prenatal VPA exposure across lemniscal and non-lemniscal circuits.

Contextual auditory-elicited responses

Next, we examined how sex, rat model, and IC division shaped neuronal responses to DEV, CAS, and STD stimuli. For each condition, we fit a generalized linear mixed-effects model that included fixed effects for IC division (lemniscal, non-lemniscal), sex (female, male), and prenatal model

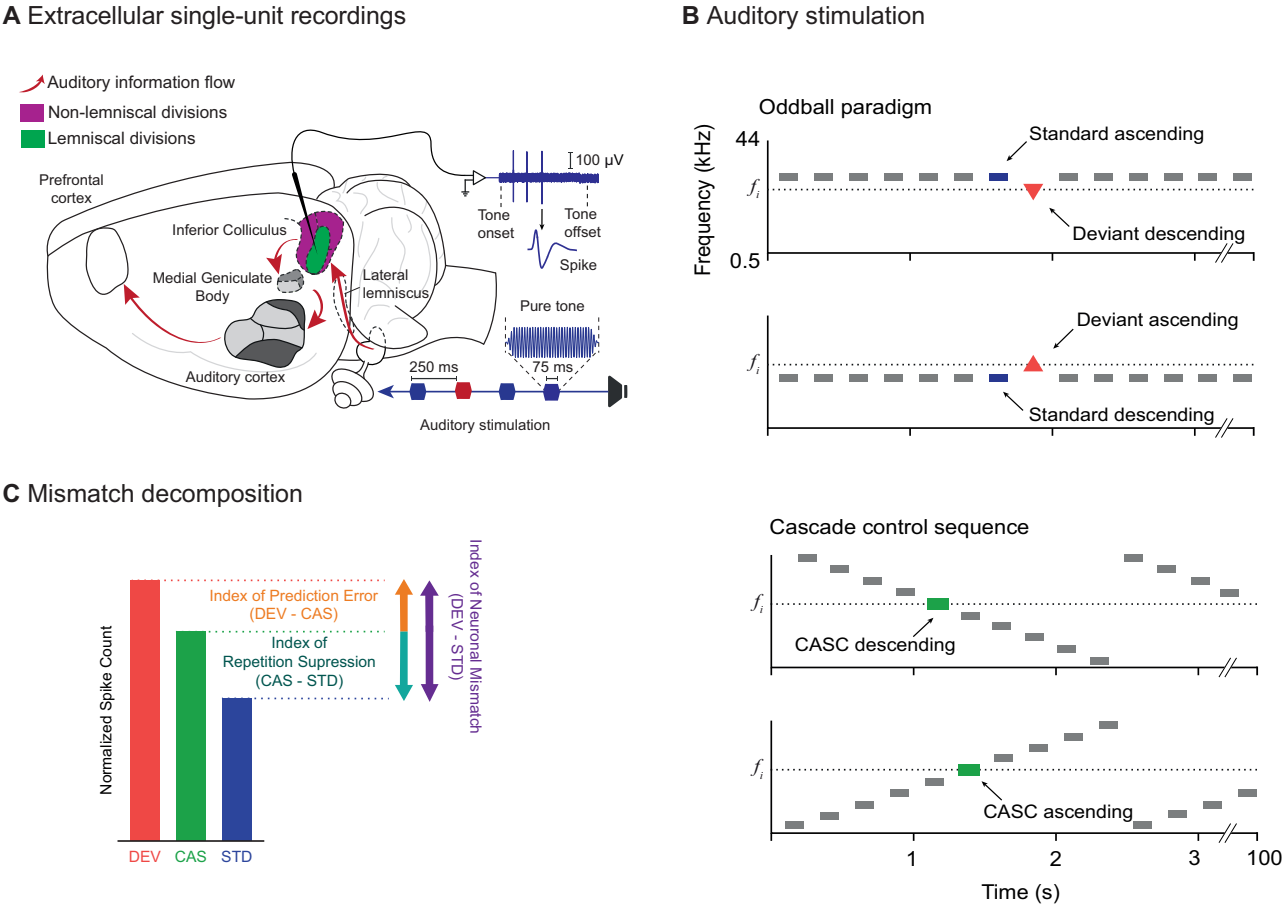

Fig. 1 | Methodology and experimental design. A Schematic of extracellular single-unit recordings in the lemniscal (green) and non-lemniscal (purple) regions of the IC in response to pure-tone auditory stimulation (red and blue). **B** Pure-tone stimulation sequences included ascending and descending versions of the classical oddball paradigm and cascade control sequences, which elicited deviant (DEV; red), cascade (CAS; green), and standard (STD; blue) responses. **C** These stimulus conditions were decomposed to compute predictive processing components: neuronal mismatch (iMM = DEV–STD), repetition suppression (iRS = CAS–STD), and prediction error (iPE = DEV–CAS). Neuronal mismatch was also obtained by summing iRS and iPE. Neuronal mismatch was also obtained by summing iRS and iPE.

(Control, *Grin2b* + /–, VPA), and all interaction terms, with random intercepts for neurons nested within animals and random slopes for IC division. This structure preserved the hierarchical organization of the dataset and allowed stimulation-evoked responses to vary appropriately across animals and IC regions. Each model included 68 division-level observations for 46 animals.

The models provided strong fits for all stimulus conditions, with intraclass correlation coefficients of 0.625 for DEV, 0.751 for CAS, and 0.702 for STD conditions. Cross-validation confirmed their predictive accuracy, yielding median absolute errors of 0.022, 0.013, and 0.030, respectively.

Together, these indices confirmed that the models captured the stable, context-dependent structure of neuronal responses across animals, sexes, and experimental groups per IC division.

Deviant-elicited responses. The deviant-elicited response reflects neuronal sensitivity to unexpected auditory events, indexing the detection of deviance within a predictable context and forming the core mismatch signal in predictive coding.

The model showed significant main effects of IC division ($p < 0.001$) and sex ($p = 0.037$) on DEV-evoked activity. It also found significant Division × Sex ($p = 0.012$), and division × VPA ($p = 0.034$) interactions (Supplementary Information, Table 3). These findings support that sex and prenatal VPA administration influenced the processing of auditory deviance in a division-specific manner.

Post hoc pairwise contrasts showed that significant effects emerged exclusively within the lemniscal IC (Supplementary Information, Table 4). Among control animals, females exhibited significantly smaller DEV-elicited responses than males (contrast estimate = –0.095, $p = 0.033$; Fig. 6A), indicating weaker auditory deviance responses in female rats. This sex-specific difference did not appear under *Grin2b* heterozygous deletion or prenatal VPA exposure. Meanwhile, DEV responses across lemniscal and non-lemniscal divisions remained unaffected across the rat model of either sex.

Cascade-elicited responses. The cascade-elicited response captures neuronal sensitivity to orderly yet non-repetitive auditory sequences, providing a control for adaptation and indexing context-driven excitability within predictive coding frameworks.

The model showed significant main effects of IC division ($p = 0.010$), sex ($p = 0.002$), *Grin2b* heterozygous deletion ($p = 0.005$), and prenatal VPA exposure ($p = 0.020$) on CAS-evoked responses (Supplementary Information, Table 3).

Post hoc pairwise contrasts revealed robust differences in CAS-evoked responses across sex and rat model within both IC divisions (Supplementary Information, Table 4). Among control animals, females showed significantly reduced CAS activity compared with males in both the lemniscal (contrast estimate = –0.169, $p = 0.001$; Fig. 6A) and non-lemniscal IC (contrast estimate = –0.093, $p < 0.001$; Fig. 6B). Among female rats, both *Grin2b* heterozygous deletion and prenatal VPA exposure increased CAS responses relative to control females in a division-dependent manner. In the lemniscal IC, CAS activity was significantly elevated in both *Grin2b* + /– (contrast estimate = –0.173, $p = 0.004$; Fig. 6A) and VPA-exposed females (contrast estimate = –0.142, $p = 0.017$; Fig. 6A).

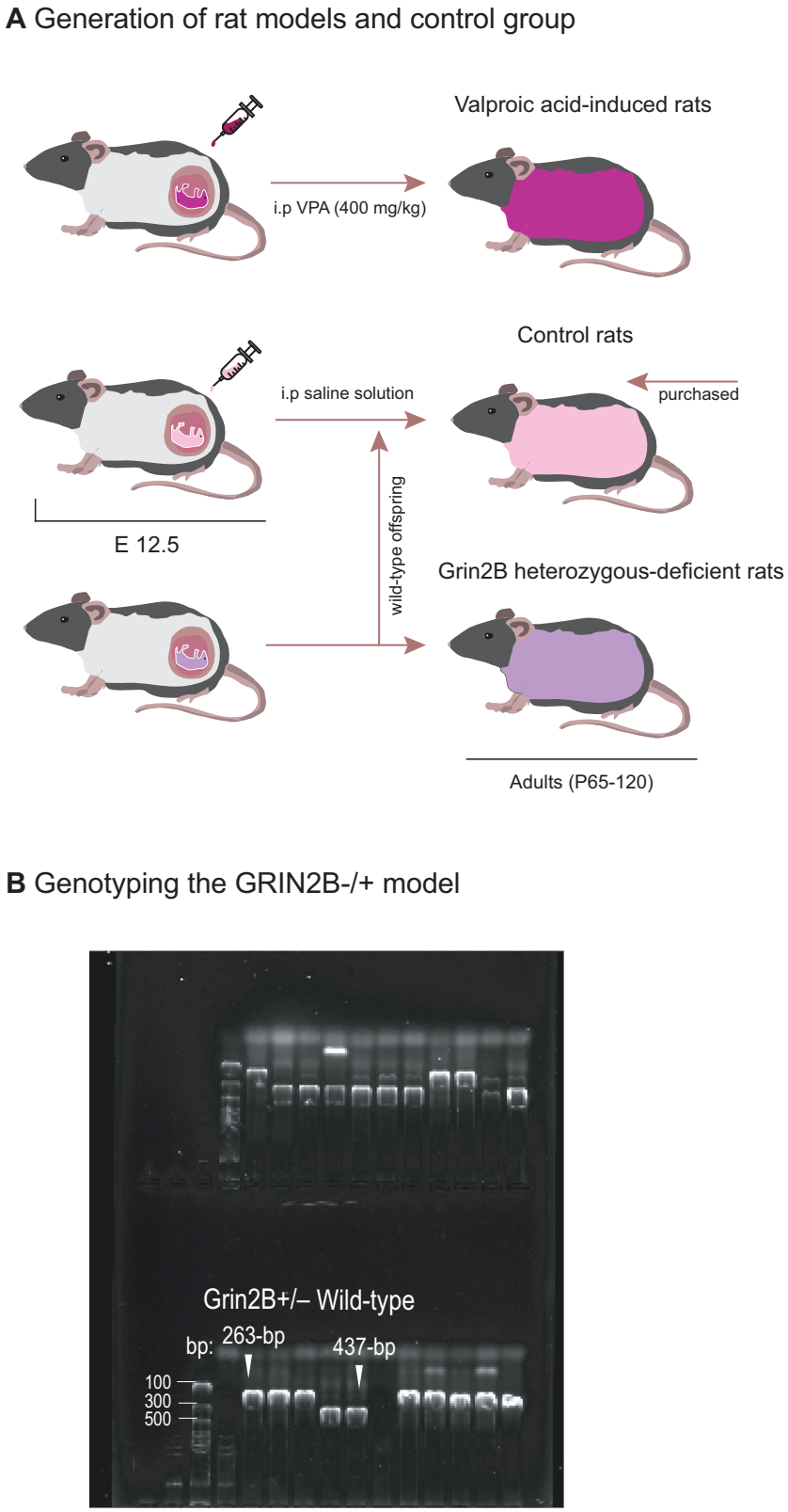

Fig. 2 | Rat model generation. A illustrates the generation of rat models. Valproic acid (VPA)–exposed rats were produced by administering an intraperitoneal injection of 400 mg/kg VPA on gestational day 12.5. *Grin2b* + /– heterozygous-deficient rats were generated by breeding wild-type females with *Grin2b* + /– males. The control cohort consisted of (i) adult animals purchased for the study, (ii) wild-type offspring from *Grin2b* + /– offspring, and (iii) pups prenatally injected with saline to control for injection-associated stress. We recorded from female and male rats at adult stages (P65–120) to assess sex- and model-dependent effects. **B** displays polymerase chain reaction genotyping results on agarose gel, confirming the presence of wild-type and *Grin2b* + /– alleles in the heterozygous-deficient model.

A similar pattern emerged in the non-lemniscal IC, where *Grin2b* + /– and VPA females again showed larger CAS responses than controls (contrast estimate = –0.080, $p = 0.008$; contrast estimate = –0.088, $p < 0.001$, respectively; Fig. 6B). In contrast, male rats did not exhibit any autism-related differences in either division.

Together, these findings show that female rats exhibit stronger IC encoding of pseudo-regular tones than males under control conditions. Regarding autism-like phenotypes, both *Grin2b* heterozygous deletion and prenatal VPA exposure dampened pseudo-regular pattern encoding in females across IC divisions, while sparing male animals.

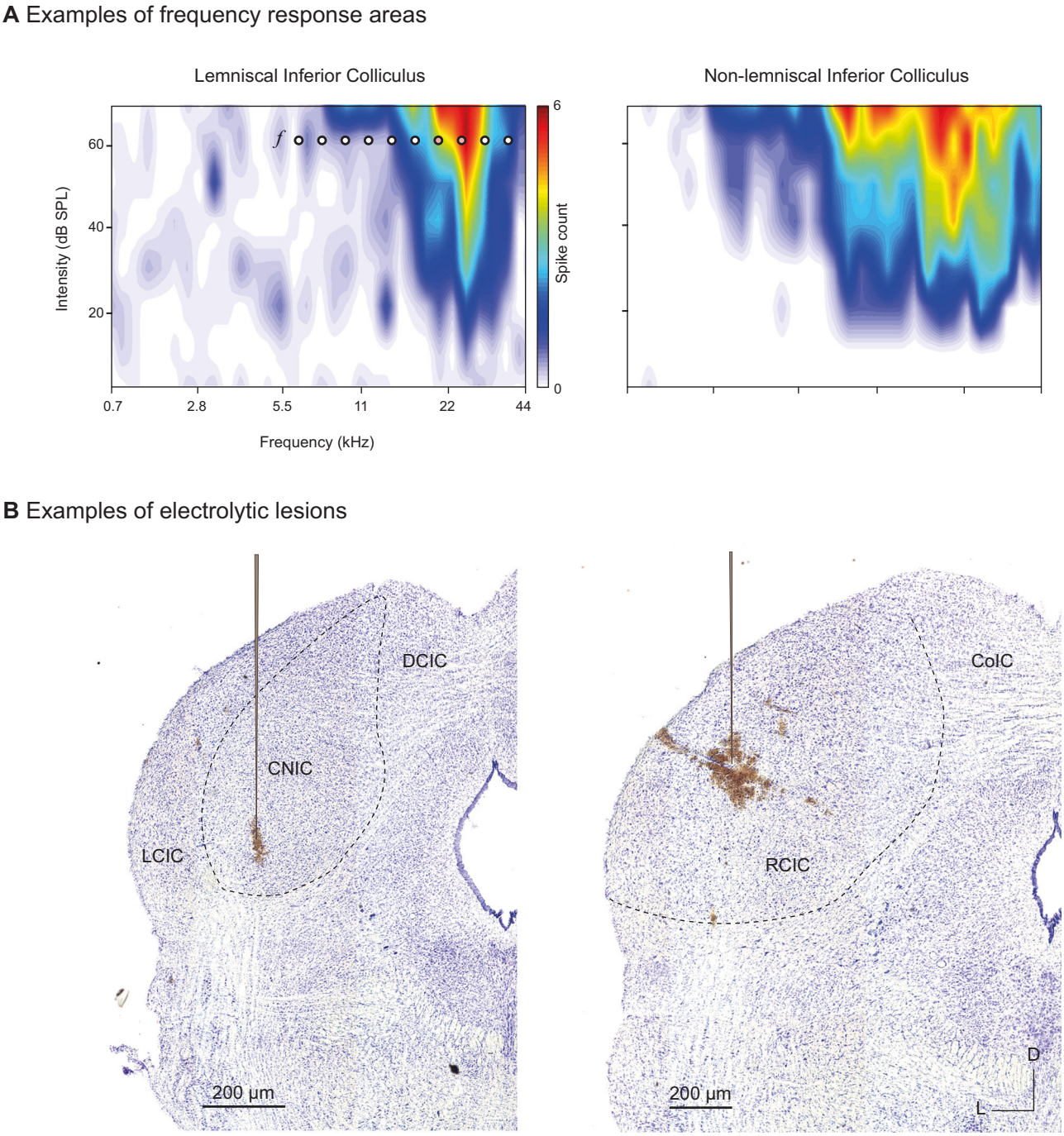

Fig. 3 | Anatomy and physiology of the lemniscal and non-lemniscal IC. **A** example of a frequency response area from the lemniscal (left) and non-lemniscal IC (right panel), with dots marking the tone frequencies used under high intensity stimulation. **B** Coronal sections of the inferior colliculus showing anatomical boundaries and representative examples of electrolytic lesions marking recording sites in lemniscal (CNIC) and non-lemniscal (DCIC, LCIC, RCIC) divisions; CoIC is the commissure of the IC; D dorsal, L lateral.

Standard-elicited responses. The standard-elicited response reflects neuronal adaptation to repetitive, predictable auditory inputs, providing a baseline measure of repetition-based encoding within the predictive hierarchy.

The model showed significant main effects of IC division ($p < 0.001$), sex ($p = 0.004$), and *Grin2b* heterozygous deletion ($p = 0.011$) (Supplementary Information, Table 3).

Post hoc contrasts showed clear sex differences in STD-evoked activity under control conditions (Supplementary Information, Table 4). Control females generated higher STD responses than control males in both the lemniscal (contrast estimate = 0.207, $p = 0.003$; Fig. 6A) and non-lemniscal IC (contrast estimate = 0.158, $p < 0.001$; Fig. 6B). Both autism-like phenotypes modulated STD responses only in females. *Grin2b* + /– females showed significantly lower STD activity relative to controls in both lemniscal (contrast estimate = 0.216, $p = 0.009$; Fig. 6A) and non-lemniscal (contrast estimate = 0.143, $p = 0.010$; Fig. 6B) IC divisions. Also, VPA females demonstrated a similar reduction in the non-lemniscal IC (contrast estimate = 0.128, $p = 0.004$; Fig. 6B). We failed to detect autism-related changes in male rats.

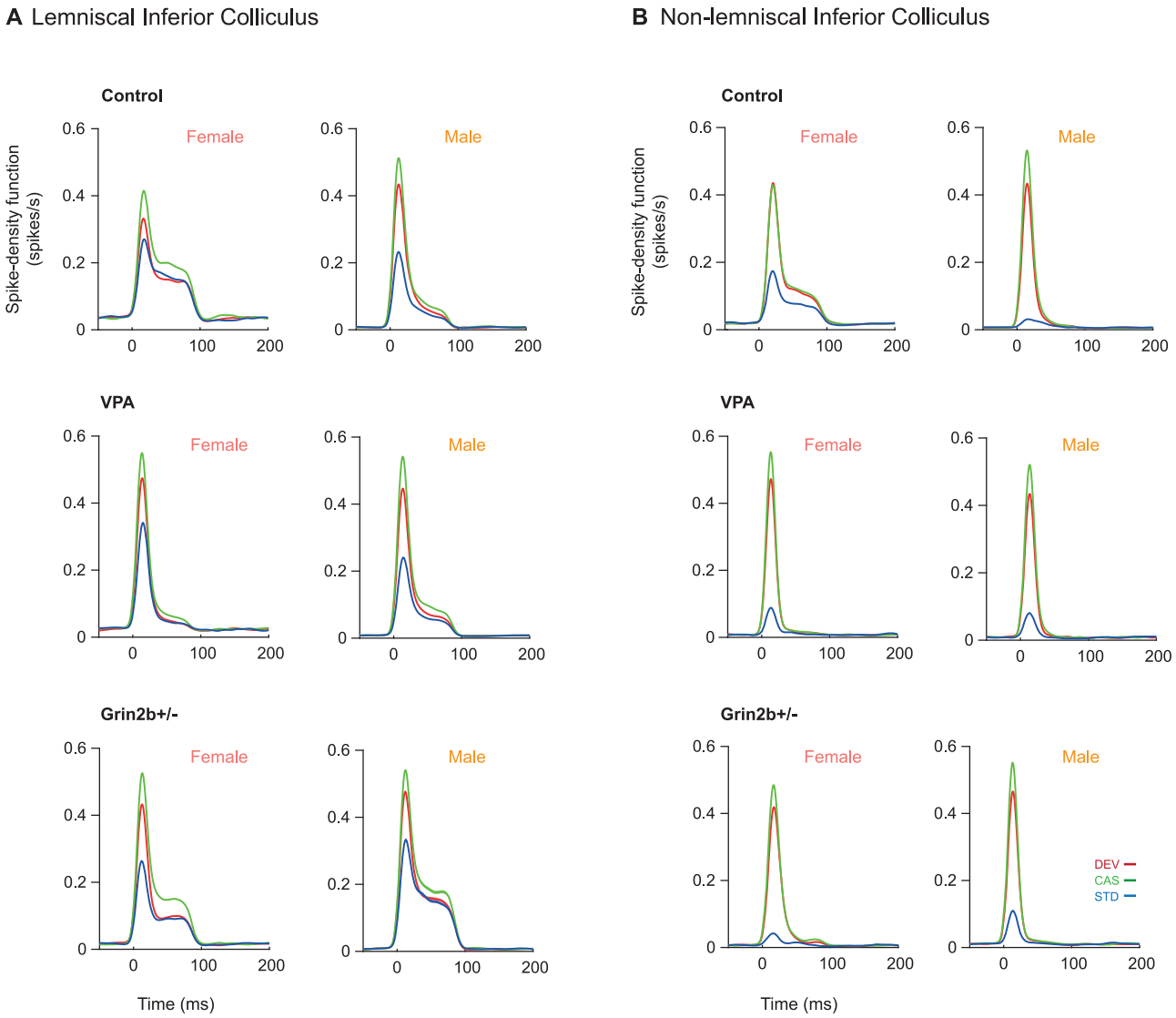

Fig. 4 | Spike-density functions across sex, rat model, and IC division. A Averaged normalized spike-density functions from lemniscal inferior colliculus neurons, aligned to tone onset and plotted for each sex and experimental group. Deviant (DEV; red), cascade (CAS; green), and standard (STD; blue) responses reveal the temporal firing profiles elicited by each condition. **B** shows the corresponding functions in the non-lemniscal division, using the same group structure and color scheme. In both panels, the traces represent population-averaged firing activity, illustrating how evoked response dynamics vary across sex, model, and IC division.

These findings show that control females exhibit higher STD-evoked activity than males, consistent with weaker repetition-based encoding. Both *Grin2b* heterozygous deletion and prenatal VPA exposure reversed this pattern in females, atypically amplifying repetition-based encoding, as reflected by reduced STD responses, with the strongest effects in the non-lemniscal IC.

Predictive components of mismatch processing

Next, we examined contextual auditory processing within the predictive coding framework by deriving mismatch-related indices (iMM, iRS, and iPE) from the corresponding contrasts among the DEV, CAS, and STD conditions.

We fitted generalized linear mixed-effects models to quantify how IC division (lemniscal, non-lemniscal), sex (female, male), and rat model (Control, *Grin2b* + /–, VPA) explained variability in the predictive components. To preserve the hierarchical structure of the data, we included random intercepts for animals and random slopes for IC division. Each model incorporated 68 division-level observations from 46 animals.

The models provided strong fits for iMM and iRS, with intraclass correlation coefficients of 0.761 and 0.854, respectively. In contrast, the iPE model yielded a lower intraclass correlation coefficient of 0.060, which aligns with theoretical expectations and our previous findings. Subcortical structures such as the inferior colliculus generate relatively small prediction error signals, particularly within lemniscal pathways, and show limited between-subject variability driven by experimental factors[32,59].

Cross-validation confirmed model performance, yielding median absolute errors of 0.037, 0.031, and 0.026 for iMM, iRS, and iPE, respectively. These results indicate that the models accurately captured hierarchical influences on predictive auditory processing across IC divisions.

Neuronal mismatch index. The neuronal mismatch index quantifies the neuron's sensitivity to auditory deviance by comparing its responses to the same tone when presented as a rare deviant versus a frequent standard. It reflects the overall mismatch signal, integrating both adaptation and prediction-related components of auditory processing.

The model revealed significant main effects of IC division ($p < 0.001$), sex ($p = 0.005$), and rat model (*Grin2b* + /–: $p = 0.034$; VPA: $p = 0.030$) on iMM (Supplementary Information, Table 5). These results indicate that iMM varied robustly across anatomical divisions, with additional modulation by sex and both autism-like conditions. The absence of significant

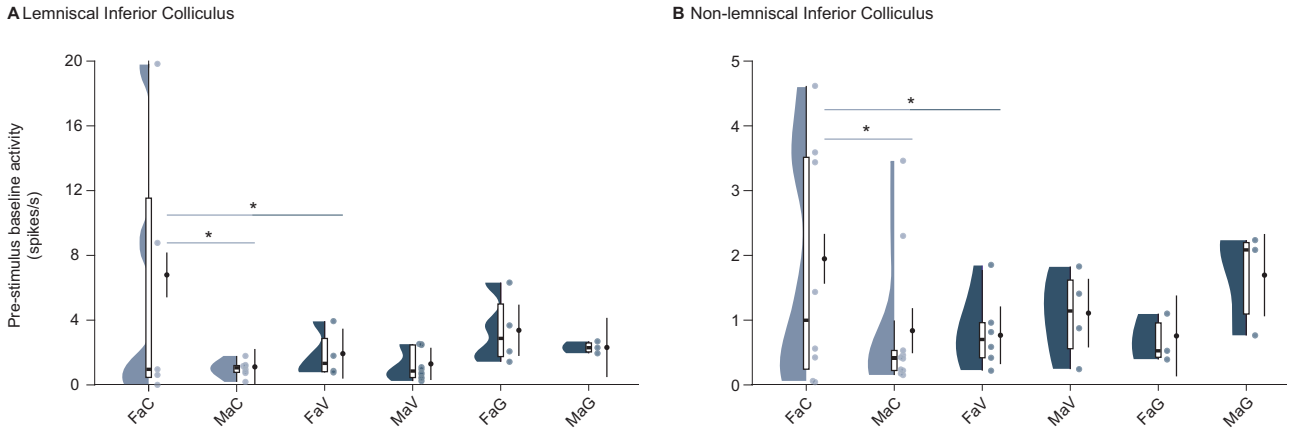

Fig. 5 | Pre-stimulus baseline activity across sex, rat model, and IC division. **A** shows half-violin plots of group-level pre-stimulus baseline activity in the lemniscal inferior colliculus. For each experimental group, the left half-violin depicts the distribution of subject-level baseline activity, with the thick black bar indicating the biological median. On the right, each dot corresponds to an individual animal, and the black circular marker denotes the estimated marginal mean with its standard error, derived from the mixed-effects model and used for statistical inference. **B** presents the corresponding baseline activity for the non-lemniscal division using the same visualization scheme. Asterisks denote significant model-based pairwise contrasts ($p < 0.05$ *, $p = 0.001$ **, $p < 0.001$ ***). Group abbreviations: *FaC* female adult control, *MaC* male adult control, *FaV* female adult VPA, MaV = male adult VPA, FaG = female adult *Grin2b* + /–, MaG = male adult *Grin2b* + /–.

interaction terms suggests that *Grin2b* heterozygous deletion and prenatal VPA exposure altered mismatch responses in a manner that was consistent across sexes and IC divisions.

Post hoc contrasts showed clear sex- and division-dependent modulation of iMM (Supplementary Information, Table 6). Under control conditions, females generated significantly smaller iMM values than males in both the lemniscal (contrast estimate = –0.310, $p = 0.003$; Fig. 7A) and non-lemniscal IC (contrast estimate = –0.157, $p = 0.007$; Fig. 7B), indicating reduced sensitivity to auditory deviance in female rats. Autism-like phenotypes altered this pattern in a sex-specific manner. Both *Grin2b* + /– and VPA-exposed females showed higher iMM than control females in the lemniscal IC (*Grin2b* + /–: contrast estimate = –0.275, $p = 0.030$; VPA: contrast estimate = –0.272, $p = 0.026$; Fig. 7A). In males, only the VPA group differed from controls, exhibiting reduced iMM in the non-lemniscal IC (contrast estimate = 0.140, $p = 0.043$; Fig. 7B).

Collectively, our results show that control females exhibited lower mismatch responses than males. Both *Grin2b* heterozygous deletion and prenatal VPA exposure atypically increased mismatch activity in females within the lemniscal IC, whereas prenatal VPA reduced mismatch responses in males within the non-lemniscal IC.

Repetition suppression index. The repetition suppression index quantifies neuronal adaptation to repeated auditory stimulation by comparing responses to standard and cascade tones, reflecting the adaptive component of predictive coding in the auditory pathway.

The model revealed significant main effects of IC division ($p < 0.001$), sex ($p = 0.004$), and *Grin2b* heterozygous deletion ($p = 0.010$) on iRS (Supplementary Information, Table 5). These results show that iRS varied across anatomical divisions and was independently modulated by sex and *Grin2b* heterozygous deficiency.

Post hoc contrasts revealed strong sex- and model-dependent modulation of iRS that occurred in both IC divisions, but with markedly larger effects in the non-lemniscal pathway (Supplementary Information, Table 6). In the lemniscal IC, control females generated significantly smaller iRS values than control males (contrast estimate = –0.345, $p = 0.003$; Fig. 7A). Among female rats, *Grin2b* heterozygous deletion further heightened iRS values relative to control counterparts (contrast estimate = –0.368, $p = 0.008$; Fig. 7A).

In the non-lemniscal IC, the pattern was stronger and more widespread. Control female animals again showed reduced iRS compared with males (contrast estimate = –0.248, $p < 0.001$; Fig. 7B). Within females, both *Grin2b* + /– and prenatal VPA-exposed rats exhibited markedly increased iRS than control females (*Grin2b* + /–: contrast estimate = –0.259, $p < 0.001$; VPA: contrast estimate = –0.220, $p < 0.001$; Fig. 7B). In contrast, neither rat model yielded significant effects in males across either IC division.

These findings demonstrate that neural suppression to repetitive stimulation is consistently lower in control females than in their male counterparts. In the autism-like models, both *Grin2b* heterozygous deletion and prenatal VPA exposure atypically amplified repetition suppression in female rats, with the strongest effects in non-lemniscal circuits.

Prediction error index. The prediction error index quantifies a neuron's capacity to signal violations of auditory regularity by isolating the deviance-related response component not explained by adaptation.

The model identified significant main effects of sex ($p = 0.005$) and *Grin2b* heterozygous deletion ($p = 0.047$) on iPE, with no significant interactions (Supplementary Information, Table 5). These results indicate that prediction error signaling in the IC varied modestly across sexes and was selectively modulated by *Grin2b* heterozygous deficiency.

Post hoc contrasts revealed clear sex differences in iPE under control conditions (Supplementary Information, Table 6). In both lemniscal and non-lemniscal IC, control females exhibited significantly higher iPE values than control males (lemniscal: contrast estimate = 0.095, $p = 0.003$; non-lemniscal: contrast estimate = 0.130, $p = 0.003$; Fig. 7A, B).

Autism-like phenotypes produced a single significant effect, confined to the non-lemniscal pathway. Prenatally VPA-exposed females showed lower iPE than control females (contrast estimate = 0.137, $p = 0.006$; Fig. 7B), whereas *Grin2b* heterozygous deletion did not alter iPE in either sex or IC division.

Our results show that prediction-error encoding is stronger in females than in males under control conditions. Prenatal VPA administration weakened female-specific effects in prediction error signaling within the non-lemniscal IC, while remaining stable in autism-like males and unaffected in lemniscal pathways.

Does short-term adaptation decay correlate with repetition suppression?

In previous studies, we evaluated half adaptation to identify the trial in which short-term adaptation showed a 50% decay in distinct animal models of psychiatric and neurodevelopmental conditions[31,59]. Here, we instead

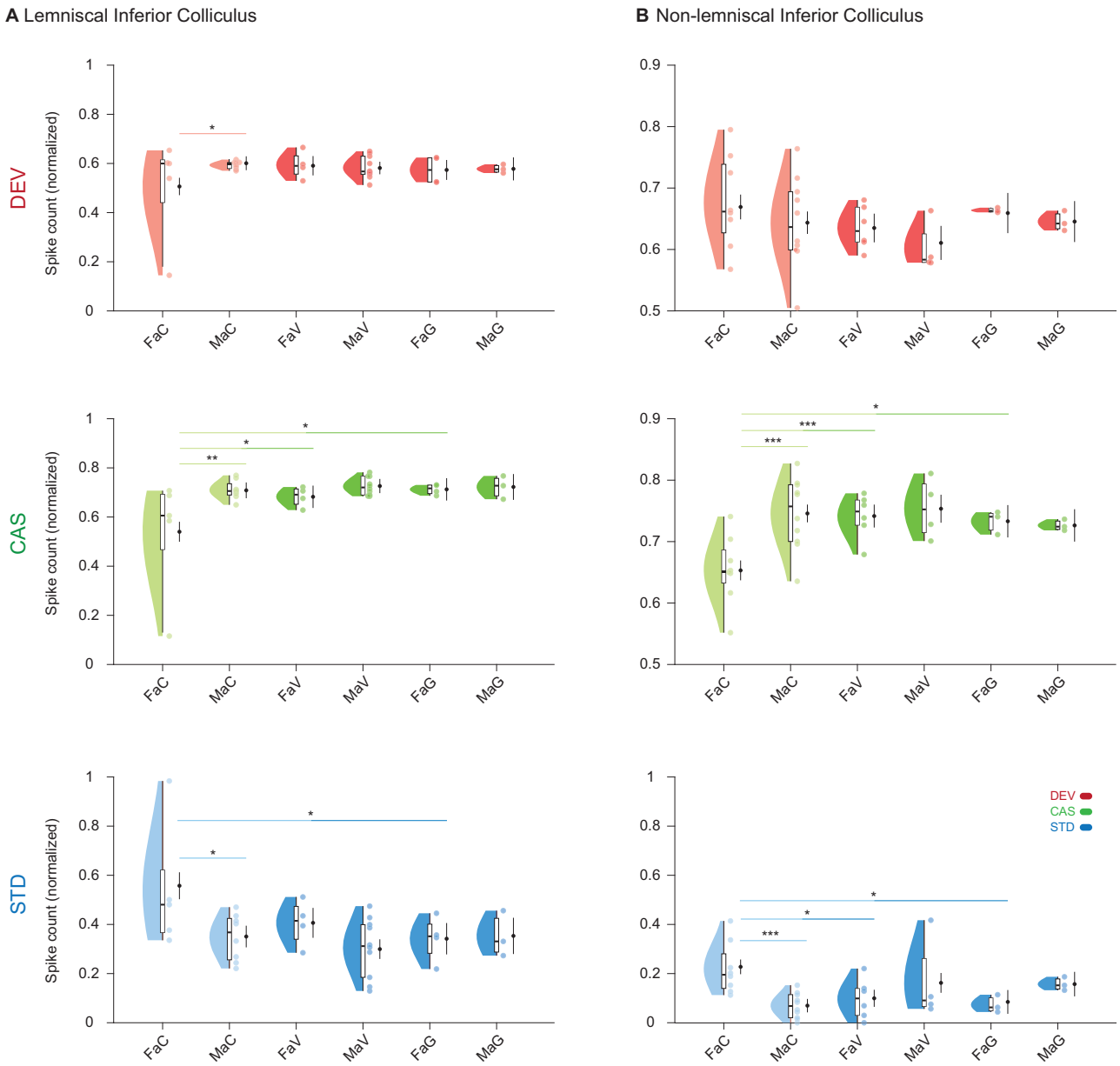

Fig. 6 | Contextual elicited responses across sex, rat model, and IC division. **A** shows half-violin plots of group-level normalized spike counts for deviant (DEV; red), cascade (CAS; green), and standard (STD; blue) responses in the lemniscal inferior colliculus; lighter shades denote control animals, whereas darker shades indicate the autism-like groups. For each experimental group, the left half-violin illustrates the distribution of subject-level spike counts, with the thick black bar marking the biological median. On the right, each dot represents an individual animal, and the black circular marker depicts the estimated marginal mean with its standard error, derived from the mixed-effects model and used for statistical inference. **B** shows the corresponding contextual responses in the non-lemniscal division using the same visualization scheme. Asterisks denote significant model-based pairwise contrasts ($p < 0.05$ *, $p = 0.001$ **, $p < 0.001$ ***). Group abbreviations: FaC female adult control, MaC male adult control, FaV female adult VPA, MaV male adult VPA, FaG female adult *Grin2b* + /–, MaG male adult *Grin2b* + /–.

characterized short-term adaptation by extracting the *b* coefficient (the adaptation exponent) from a power-law fit to the first 10 STD trials (Fig. 8A), which illustrates the distribution of adaptation rates used for subsequent correlation analyses. This parameter captures the rate at which neuronal responses decay across repeated stimulation, with more negative values indicating faster adaptation. Then, we examined whether the rate of short-term adaptation, quantified by the adaptation exponent (*b*), was associated with the degree of repetition suppression (iRS) using Spearman correlation analysis across experimental groups (Fig. 8B).

Spearman correlation analyses with false discovery rate correction (Fig. 8B) showed that only *Grin2b* + /– male rats in the lemniscal IC division exhibited a strong negative association between short-term adaptation and neural suppression during stimulus repetition ($p < 0.001$). In the non-lemniscal IC division, control males and females showed weak but significant negative correlations ($p < 0.001$), consistent with a preserved adaptive scaling. This relationship was stronger in both sexes of the prenatally VPA-induced group ($p < 0.001$), indicating heightened repetition sensitivity. *Grin2b* + /– male rats also maintained a significant association in the non-lemniscal pathway ($p = 0.012$), whereas *Grin2b* + /– female rats lack this correlation, suggesting a disruption in the typical coupling between short-term adaptation decay and suppression of neuronal activity upon repetitive stimulation.

Discussion

We investigated pre-stimulus baseline activity and context-evoked responses in the lemniscal and non-lemniscal IC to determine how sex

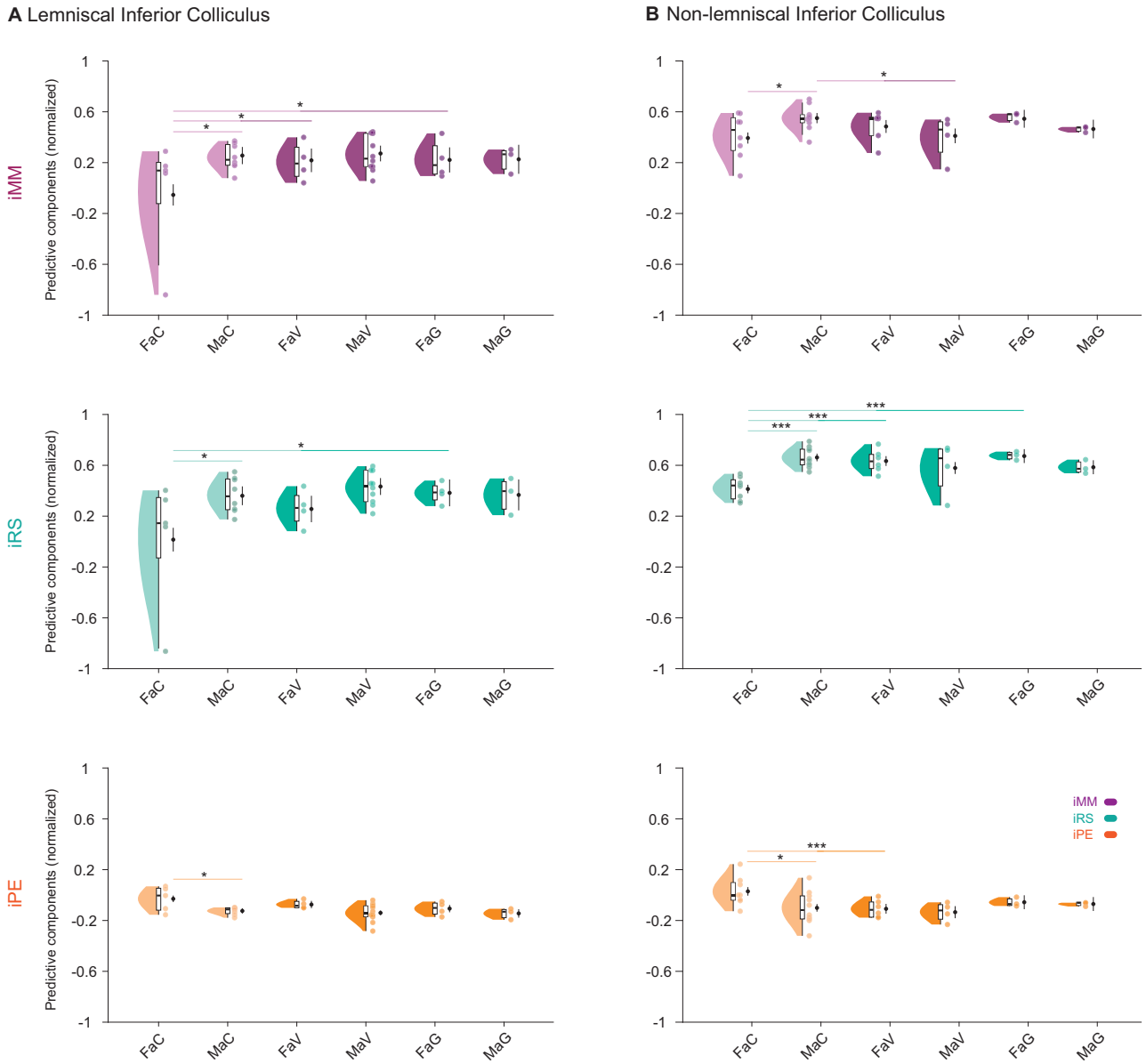

Fig. 7 | Predictive components of mismatch processing across sex, rat model, and IC division. A shows half-violin plots of group-level normalized spike counts for the neuronal mismatch (iMM; purple), repetition suppression (iRS; turquoise), and prediction error (iPE; orange) components in the lemniscal inferior colliculus. Lighter tones represent control animals, whereas darker tones indicate the autism-like groups. For each experimental group, the left half-violin depicts the distribution of subject-level component values, with the thick black bar marking the biological median. On the right, each dot corresponds to an individual animal, and the black circular marker indicates the estimated marginal mean with its standard error, derived from the mixed-effects model and used for statistical inference. **B** presents the corresponding predictive components in the non-lemniscal division using the same visualization scheme. Asterisks denote significant model-based pairwise contrasts ($p < 0.05$ *, $p = 0.001$ **, $p < 0.001$ ***). Group abbreviations: FaC female adult control, MaC male adult control, FaV female adult VPA, MaV male adult VPA, FaG female adult *Grin2b* + /–, MaG male adult *Grin2b* + /–.

and autism-like phenotypes modulate predictive processing. Our central finding is the existence of a sex-specific organization of predictive processing in the auditory midbrain, expressed across control and autism-like conditions and revealed at the level of distinct predictive components.

Our analytical approach differs from our previous study[59], which characterized contextual modulation using direct neural recordings and descriptive statistics in control and VPA rats. In the present study, we implemented hierarchical mixed-effects models and report model-based contrast estimates that account for subject-level variability and interactions between sex, model, and IC division. This approach is increasingly recommended for nested neural datasets[60] and for interpreting structured contrasts in mixed models[61].

This shift in statistical framework naturally results in numerical differences in estimated effects and significance patterns relative to our earlier analyses[59], while providing new mechanistic insights. The contrast estimates reported here quantify the modeled effects of autism-relevant perturbations on the computational structure of IC processing, whereas the earlier descriptive work captured the expressed neural phenotype at the level of empirical spike rates and trial-based averages.

Together, these complementary perspectives provide a multilevel account of auditory midbrain function: one describing what neurons express during contextual stimulation, and the other explaining how predictive computations are differentially organized across sex and autism-like conditions.

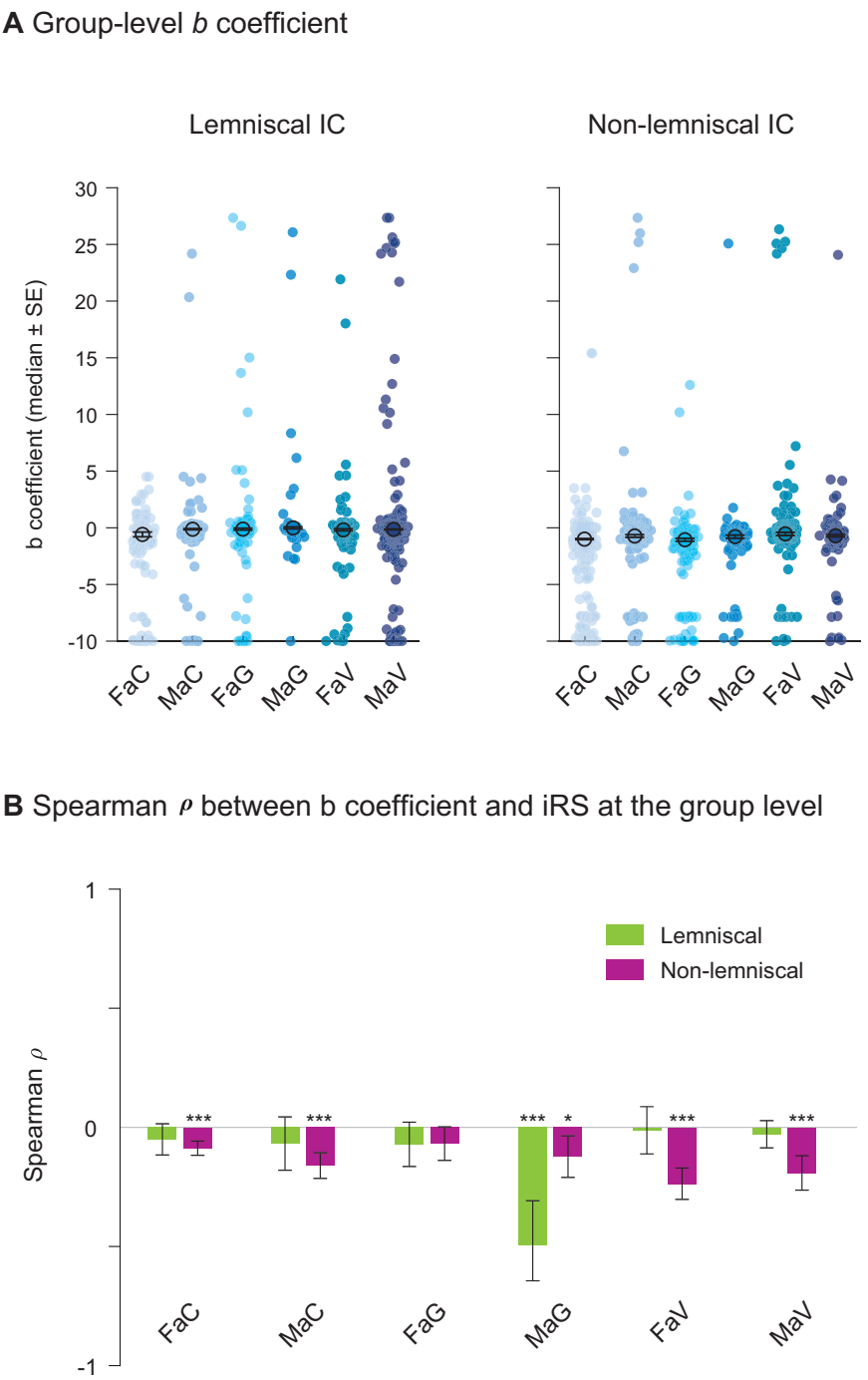

Fig. 8 | Spearman correlation between short-term adaptation and repetition suppression across control and autism-like rat models in the IC. **A** Scatter plot showing group-level medians of the *b* coefficients, derived from power-law fits to the first 10 standard trials per animal, separately for the lemniscal (left) and non-lemniscal (right) divisions of the IC. **B** Spearman correlations between the *b* coefficient and iRS across control and autism-like rat groups in lemniscal (green) and non-lemniscal (purple) regions. The asterisks indicate statistical significance: $p < 0.05$ *, $p = 0.001$ **, and $p < 0.000$ ***. Group abbreviations: FaC = female adult control, MaC male adult control, FaV female adult VPA, MaV male adult VPA, FaG female adult *Grin2b* + / –, MaG = male adult *Grin2b*++/–.

Summary

In conceptual terms, our results show that neuronal processing of pre-stimulus baseline activity and auditory stimulus context in the IC depends on interactions among sex, circuit division, and autism-relevant neurodevelopmental perturbations. Under control conditions, female rats exhibited higher pre-stimulus baseline activity than males across IC divisions, indicating a sex-biased tonic excitability state prior to sound onset. Prenatal exposure to VPA selectively reduced this elevated baseline activity in females, whereas heterozygous deletion of *Grin2b* did not alter baseline activity in either sex. At the level of stimulus context, control females showed weaker sensitivity to deviant sounds, reduced responses to orderly non-repetitive sequences, and higher responses to repeated standards than males, reflecting sex-specific encoding of regularity, repetition, and deviance. Autism-linked risk factors modified these responses in opposite directions across sexes: females exhibited increased mismatch-related responses driven by enhanced repetition suppression and reduced prediction-error signaling, whereas males showed weaker and more restricted reductions in mismatch responses. These effects were strongest in non-lemniscal circuits.

Together, these findings indicate that autism-relevant genetic and environmental perturbations reshape predictive components of context-dependent auditory processing in a sex- and circuit-specific manner, rather than producing a uniform change in auditory responsiveness.

Sex and autism-like effects on pre-stimulus baseline activity within the IC

Our findings revealed a sex-dependent organization of pre-stimulus baseline activity within the IC. Under control conditions, female rats consistently showed higher baseline activity than males across both IC divisions.

Although direct evidence on sex differences in spontaneous neural activity remains limited, human work suggests that female auditory pathways operate with intrinsically higher functional gain. Women exhibited stronger activation of the primary auditory cortex and reduced deactivation of attentional networks during sound processing[62], also usually displaying earlier and larger auditory brainstem and midbrain responses[63]. These evoked signatures point to an auditory system that is more responsive at baseline. Broader neuroimaging data support this interpretation. Positron emission tomography and perfusion imaging studies report higher resting cerebral blood flow and metabolic activity in women across widespread cortical regions[64,65].

Taken together, these findings support a biologically coherent framework in which female sensory circuits operate at a higher basal activation state, consistent with the elevated pre-stimulus activity observed in our control animals.

Beyond the sex differences observed under control conditions, our analysis revealed that autism-like phenotypes modulated pre-stimulus baseline activity in a strongly sex-dependent manner. Prenatal VPA exposure reduced spontaneous firing predominantly in females, with the most pronounced effects emerging in the non-lemniscal inferior colliculus. This division is classically associated with context sensitivity, prediction updating, and deviance tracking[66], suggesting that female circuits may be especially vulnerable to disruptions in intrinsic excitability within prediction-related pathways. In contrast, males showed remarkably stable baseline activity across both models.

Evidence for alterations in spontaneous or resting neural activity across autism models is mixed and strongly circuit-dependent. For instance, cortical neurons of the Fmr1 knockout mice often display heightened intrinsic excitability, particularly in layer 5 pyramidal neurons of the primary somatosensory cortex[67]. Other monogenic models such as Cntnap2 and Shank3 exhibit divergent disruptions in intrinsic activity and network organization. In Cntnap2 knockout mice, layer 5 pyramidal neurons in the medial prefrontal cortex exhibit reduced spontaneous firing[68], whereas somatosensory cortical circuits show network hyperexcitability driven by diminished interneuron activity[69]. Shank3B −/− mice exhibit early corticostriatal hyperactivity and abnormal maturation in striatal circuits[70]. Human studies reveal similar heterogeneity: while some autistic individuals exhibit sensory hypo-responsiveness and reductions in resting-state neural activity in specific cortical regions, others show elevated baseline activity or hyper-connectivity depending on developmental stage and neurocognitive network[71].

The decreases in pre-stimulus baseline firing that we observed in VPA-exposed females likely reflect a selective reorganization of intrinsic excitability within auditory midbrain circuits, rather than a generalizable feature of autism.

Sex-specific effects in predictive processing under control conditions within the IC

We quantified predictive processing at the single-neuron level by evaluating iRS, iPE, and iMM under high-intensity stimulation, which reliably elicits context-driven modulation across sex and rat model and aligns with the supra-threshold auditory stimulation commonly used in human autism research.

Across predictive components, sex exerted a robust, yet divergent influence under control conditions. Male rats showed greater iRS than females in both lemniscal and non-lemniscal IC, indicating stronger repetition-based encoding of auditory regularity. In contrast, iPE was significantly higher in females, demonstrating stronger prediction-error signaling when deviance violated the expected stimulus structure. These divergent tendencies converged in the composite iMM index. Because iMM reflects the balance between repetition suppression and prediction error, control females ultimately exhibited lower iMM than males across both IC divisions.

Together, these patterns reveal a sexually differentiated organization of predictive processing in the auditory midbrain of Long-Evans rats: males bias toward more stable encoding of regularity, whereas females generate larger mismatch-related error signals. This dissociation indicates that predictive components are not simply scaled by overall excitability, but instead represent distinct computational processes with their own sex-dependent biases.

Human studies on typical sex differences in repetition suppression have yielded inconsistent results, often based on event-related components such as N1, P2, N2, or mismatch negativity. For example, males show greater N170 attenuation to repeated faces[72] and enhanced N2 responses to tones[73], suggesting stronger adaptation and attentional responses to novelty. Conversely, females exhibit greater P2 amplitudes regardless of the emotional salience of auditory stimuli[73], and tend to show heightened novelty responses in emotionally salient contexts.

Although these results vary with task, developmental stage, and stimulus context, they resonate with the dual pattern observed here: males favor predictive stability through stronger regularity encoding, whereas females generate stronger responses to violated expectations.

Sex-divergent predictive processing and potential non-lemniscal IC vulnerability in autism models

The predictive coding framework posits that perception emerges from the dynamic balance between internally generated predictions and incoming sensory signals[25]. In autism, this balance may diverge across sexes, leading to distinct computational phenotypes. Within this framework, both prenatal VPA exposure and *Grin2b* heterozygous deletion produced parallel, sex-specific alterations in auditory predictive processing, particularly within the non-lemniscal IC, where contrast estimates consistently revealed the strongest model effects.

In female rats, both prenatal VPA exposure and *Grin2b* heterozygous deletion increased iMM within the lemniscal IC. In the non-lemniscal division, VPA-exposed females showed reduced iPE, consistent with weakened deviance-related prediction-error signaling. *Grin2b* heterozygous-deficient females exhibited a marked increase in iRS across both divisions, with prenatal VPA producing a similar increment specifically within the non-lemniscal pathway.

In male rats, atypical predictive processing was confined to the VPA model. Prenatal VPA exposure significantly reduced iMM in the non-lemniscal IC, indicating dampened mismatch sensitivity, while sparing lemniscal responses. Neither prenatal VPA administration nor *Grin2b* heterozygous deletion altered iRS or iPE in males.

One could argue that the stronger iMM observed in autism-like female rats may reflect compensatory top–down modulation or an exaggerated influence of internal models, in line with reports of greater reliance on cognitive strategies and camouflaging behaviors in autistic females[74,75]. By contrast, the weaker iMM in autism-like male rats may indicate a stronger dependence on bottom–up sensory processing, consistent with a reduced contextual modulation frequently described in autistic males[76]. Because we obtained our results at the subcortical level, these interpretations remain tentative, and there is a clear need to assess these sex-divergent mechanisms throughout the auditory hierarchy and across translational autism-like models and human studies.

Our findings also contribute to a growing body of evidence implicating the non-lemniscal, or non-classical, auditory pathway in the neurobiology of autism[77]. This evolutionarily conserved system projects not only to auditory structures but also to limbic, paralimbic, and autonomic regions, influencing arousal regulation, emotional salience, and multisensory integration[45,78–81]. During typical development, the influence of this pathway diminishes as cortical hierarchies mature, and top–down control strengthens[82]. In autism, however, the non-lemniscal system may remain hyperactive or developmentally delayed, contributing to increased sensory gain, heightened emotional reactivity, and impaired filtering of irrelevant stimuli[77].

Structural and functional alterations in autism models

While previous studies have shown that prenatal VPA exposure disrupts auditory structure and function[83–92], and the *Grin2b* +/– model exhibits

abnormalities across various brainstem regions[93], its subcortical auditory circuits remain underexplored. The *Grin2b* gene encodes the NMDA receptor subunit ε2 and is broadly expressed during embryogenesis[94], but becomes restricted to the forebrain postnatally[95], where it plays a critical role in synaptic plasticity, learning, and memory[93,96–98]. Previous investigations into the biological mechanisms altered in these autism-like rat models revealed that the two induced opposite shifts in excitatory–inhibitory circuitry, yet converged on similar sex-dependent outcomes, as observed in the present study.

Heterozygous deletion of *Grin2b* weakened NMDA receptor–mediated currents and long-term depression, shifting cortical networks toward hypo-excitation and reduced synaptic plasticity throughout postnatal development[93,97,99]. In contrast, prenatal VPA exposure markedly increased excitatory tone by enhancing glutamatergic transmission in the dorsal raphe nucleus[100], promoting hyper-connectivity among neocortical pyramidal neurons[101], increasing excitability and long-term potentiation in amygdala pyramidal neurons[102], and upregulating post-synaptic cell adhesion molecules such as neuroligins and neurexins[103,104], all of which contributed to an elevated excitatory–inhibitory ratio across multiple brain regions. But sex-specific differences in excitatory–inhibitory balance within each rat model remain unexplored.

Despite these anatomically and functionally divergent circuit profiles, both autism models exhibited a common outcome: sex-specific alterations in predictive processing mostly localized to the non-lemniscal IC. This shared pattern suggests that biological sex critically influences the emergence of divergent predictive states, hyper-precise in females and hypo-precise in males. These findings underscore the importance of sex as a key experimental variable when evaluating autism-related phenotypes across monogenic and teratogenic models. By comparing both prenatally VPA-induced and *Grin2b* + /– rat models, we identified shared disruptions in early predictive coding, despite differences in molecular etiology and global circuit architecture.

Within the predictive coding framework, over-weighted predictions can suppress bottom-up input[26,105], resulting in elevated iRS and diminished iPE as observed in our autism-like female rats. This imbalance yields an iMM signal driven more by exaggerated adaptation than by deviance detection. Conversely, in autism-like males, reduced iMM without compensatory increases in iPE reflects under-weighted predictions[29,106]. This failure to effectively constrain sensory input produces a weakened mismatch response and impaired encoding of contextual regularities. Together, these findings support that sex-specific modulation of subcortical prediction weights may give rise to divergent neurocomputational profiles of sensory inference in autism.

Methodological considerations

An important consideration in our study is that recordings were conducted under anesthesia, which can affect physiological activity by dampening certain neural dynamics[107,108] while preserving overall network responsiveness[109]. Indeed, urethane is widely used in auditory neurophysiology and preserves essential aspects of spontaneous and evoked activity[110,111], including predictive responses[32,50], it precludes the assessment of state-dependent modulation and prevents direct links between altered predictive indices and behavior. Therefore, while the single-neuron differences we observed may underlie predictive coding disruptions relevant to autism-like traits, this interpretation remains tentative in the absence of behavioral correlation.

Nonetheless, our findings offer a robust neural framework for understanding sex- and model-specific disruptions in predictive processing and lay the groundwork for future studies in awake, behaving animals to bridge the gap between circuit-level alterations and cognitive phenotypes.

Methods

Animal housing and ethical compliance

We conducted single-unit recordings on *Grin2b* + /– (female $n = 4$; male $n = 3$), VPA (female $n = 7$; male $n = 11$), and control (female $n = 11$; male $n = 10$) Long-Evans rats at young adulthood (postnatal days 65–120) stages[112]. We housed the animals in pairs or trios matched by sex and model in ventilated cages under a 12-hour light/dark cycle, with *ad libitum* access to food and water.

We have complied with all relevant ethical regulations for animal use. Experimental procedures conformed to the guidelines of the Directive of the European Communities (86/609/EEC, 2003/65/EC and 2010/63/EU) and RD 53/2013 Spanish Legislation for the use and care of animals. The Bioethics Committee of the University of Salamanca approved all study details (USAL-ID-195 and USAL-ID-574).

VPA-induced rat model

To generate the prenatally VPA-induced offspring (Fig. 2A), we mated five control male and female rats overnight until vaginal smear cytology confirmed gestational day 0. We administered an intraperitoneal injection of 400 mg/kg VPA to pregnant females on gestational day 12.5[113,114]. The solution consisted of 250 mg/mL sodium valproate in 0.9% saline. We monitored the pregnancies until delivery and weaned prenatally VPA-exposed littermates on postnatal days 21–23.

We selected VPA-exposed offspring from four independent litters. From the first litter, we included one female and three male pups; from the second, three female and two male pups; from the third, two female and three male pups; and from the fourth, one female and three male pups. Each litter contributed animals of both sexes, and no litter dominated the sample. This distribution reduced the likelihood that litter-specific factors, rather than prenatal exposure, drove group differences.

We conducted single-unit recordings on the offspring with simple tail malformations, as previous studies have identified these as markers of VPA teratogenicity during embryonic neural development[115–118].

Grin2b + /– rat model

For the *Grin2b* + /– rat model (Fig. 2A), we purchased three male rats carrying a heterozygous deletion in the *Grin2b* gene (Rat Strain Long-Evans-*Grin2b*em1Mcwi) from the Medical College of Wisconsin (Gene Editing Rat Resource Center, United States). This mutation involves a deletion of exon 3, introduced by CRISPR/Cas9 system in the *Grin2b* gene of Crl:Long-Evans rat embryos. Importantly, the Simons Foundation Autism Research Initiative (SFARI) supported the generation of this rat model in the Gene Editing Rat Resource Center.

We bred the three *Grin2b* + /– males with three control female rats housed in our animal care facility and genotyped the offspring to confirm the presence of the heterozygous mutation in the *Grin2b* gene. We performed genotyping using polymerase chain reaction (PCR) according to the protocol provided by the Gene Editing Rat Resource Center. We collected tail tissue, extracted DNA with the DNeasy Blood & Tissue Kit (Qiagen), and amplified the DNA using PCR Master Mix (Thermo Fisher Scientific). We used the forward primer GGATTCCAAGCACAAAGTCTCCT and the reverse primers CTCCTGCCCTACTGTGAGCTTGG and CCAAACTGGAAGAACATGGAGG. Our PCR protocol began with a 95°C hold for 5 minutes, followed by 35 cycles at 95°C for 30 seconds, 60°C for 30 seconds, and 68°C for 45 seconds, ending with a final extension at 68°C for 5 minutes and a 4°C hold. We analyzed the samples on a 2% agarose gel to visualize DNA fragments to distinguish heterozygous *Grin2b* deletions. Control rats showed a 437-bp band, while *Grin2b* + /– animals displayed a 263-bp band (Fig. 2B).

We selected *Grin2b* heterozygous deleterious mutants from three independent litters. From the first litter, we included one male and two female pups; from the second, one male and one female pups; and from the third, one male and one female pups. This distribution limited the potential impact of litter origin on the statistical analysis.

Control rat model

The control group consisted of male and female typically developing adult rats, organized into three cohorts designed to match the requirements of both the genetic and environmental autism-like models.

Control animals included: (1) sixteen rats purchased from Janvier; (2) three rats of pregnant females injected intraperitoneally with 0.9% saline on gestational day 12 and weaned between postnatal days 21–23, to control for potential stress effects associated with intraperitoneal injection in the VPA design; and (3) two rats resulting from breeding heterozygous *Grin2b* mutants with wild-type rats, a litter independent from the litters used for the *Grin2b* + /– generation (Fig. 2A).

After assessing single-unit recordings, we found that sex-matched purchased and in-house-born rats exhibited no significant differences in contextual processing using *ranksum* function with Bonferroni correction ($p > 0.05$). Therefore, we pooled data from both groups to form the main control rat group, treating female and male animals separately for pairwise comparisons.

Surgical procedures

Surgical and recording procedures followed established protocols[32]. Anesthesia was induced with urethane (1.5 g/kg, i.p.), with supplemental doses (~0.5 g/kg) administered as needed to maintain a deep anesthetic plane. Urethane was selected for its minimal and balanced effects on inhibitory and excitatory synapses, preserving neural activity more faithfully than other agents[50,110,111,119].

Normal hearing was confirmed in all rats (Control, *Grin2b* + /–, and prenatal VPA administration) using auditory brainstem responses recorded subcutaneously with subdermal needle electrodes. Auditory brainstem responses were acquired with an RZ6 Multi I/O Processor and processed using BioSig software (Tucker-Davis Technologies). Click stimuli (0.1 ms, 21 clicks/s) were delivered monaurally to the right ear in 10 dB steps (10–90 dB SPL) via a Beyer DT-770 earphone fitted with a custom cone and tube. Auditory thresholds did not differ significantly across groups, as assessed by Wilcoxon ranksum tests in MATLAB.

Following hearing assessment, a tracheal cannula was inserted to support ventilation, and expiratory CO_2 was monitored due to urethane's respiratory depressant effects. Body temperature was maintained at 37 ± 1°C using a rectal probe and homeothermic blanket (Cibertec). The head was secured in a stereotaxic frame with hollow specula replacing ear bars; the right speculum housed the sound delivery system. Ophthalmic gel protected the eyes.

To stabilize physiology, we administered atropine sulfate (0.1 mg/kg, s.c.) to reduce secretions, dexamethasone (0.25 mg/kg, i.m.) to limit brain edema, and 5 ml of subcutaneously injected glucosaline to prevent dehydration. The low doses used for atropine and dexamethasone injections have no reported effects on central auditory processing or neuronal excitability at the level of the inferior colliculus.

After shaving and disinfecting the scalp, we made a midline incision and retracted the periosteum to expose the parietal and rostral occipital bones. A craniotomy was performed over the caudal left parietal bone, exposing the cortex above the left IC. The dura was removed, and the surface was covered with 2% agar to prevent drying during recording.

Single-neuron electrophysiological recordings

We recorded extracellular activity from single neurons in the left IC using glass-coated tungsten microelectrodes (1.5–3.5 MΩ at 1 kHz) following established protocols[31,32,56,59,120]. Experiments were conducted in a sound-insulated, electrically shielded chamber. Electrodes were inserted at a 20° rostral angle using a piezoelectric micromanipulator (Sensapex), targeting units responsive to auditory stimuli.

Auditory stimuli were generated with an RZ6 Multi I/O Processor (Tucker-Davis Technologies) using OpenEx software and MATLAB. White noise bursts and 75 ms pure tones (5 ms rise-fall ramps) were used for single-unit isolation. Experimental protocols employed only pure tones, delivered monaurally at 4 Hz through a calibrated close-field earphone (Beyer DT-770) covering 0.5–45 kHz with flat output up to 76 ± 3 dB SPL. All stimuli presented were sinusoidal pure tones of 75 ms duration, including 5 ms raise-fall ramps.

Neural signals were digitized at 12 kHz, amplified (251×), and filtered (0.5–3 kHz). Spike detection used a manual threshold (~2–3 SD above baseline), and single units were identified based on waveform consistency and signal-to-noise ratio (>5).

$$\text{Signal/Noise Ratio} = \frac{\max(\bar{x}(\text{waveforms})) - \min(\bar{x}(\text{waveforms}))}{\text{Std(waveforms)}}$$

We first mapped each neuron's frequency response area using randomized presentations of tones (0.7–44 kHz, 3–5 repetitions). Based on the FRA, we selected 10 pure tones spaced 0.5 octaves apart, ensuring at least two consecutive tones fell within the excitatory region (Fig. 3A). These tones were used to construct both oddball and cascade control (CAS) sequences.

The oddball paradigm consisted of frequent standard (STD) tones and rare deviants (DEV; 10% probability), with at least three STDs preceding each DEV, whose difference results in the mismatch response[32,121]. Only the final STD before each DEV was analyzed. DEV tones were pseudorandomly distributed across the sequence, and the first 10 tones were always STD. This structure yielded approximately 40 trials per condition (DEV, STD) for each tone of interest. This is similar for the CAS stimuli.

Each sequence contained 400 tones delivered at 4 Hz and fixed intensity (typically 40–70 dB SPL), with repeated recordings at different intensities when signal stability permitted. Sequence order was pseudorandomized across trials.

Each oddball and CAS sequences were presented with both ascending and descending versions, at one or more intensities depending on recording duration and signal quality. Presentations at different levels followed no specific order. In rare cases where recording stability allowed, multiple sets were acquired. When signal quality dropped below the threshold, the recording was stopped, and incomplete sets were discarded.

This design enabled decomposition of mismatch responses (iMM = DEV – STD) into repetition suppression (iRS = STD–CAS) and prediction error (iPE = DEV – CAS). While iMM can arise from frequency-specific adaptation to STD tones, only a stronger DEV response relative to CAS supports the presence of prediction error signaling. If DEV ≤ CAS, the mismatch can be fully attributed to adaptation; if DEV > CAS, prediction error mechanisms are inferred (Fig. 1C)[32,122].

A key limitation of neuronal mismatch measurements in the oddball paradigm is that PE-related activity cannot be dissociated from lower-order effects such as frequency-specific adaptation[123,124]. Control sequences are therefore required to estimate the relative contribution of these higher- and lower-order processes to the overall mismatch response[58]. To achieve this, control tone sequences must (1) include the same tone of interest with the same presentation probability as the DEV (10%), (2) maintain an equivalent stimulation rate (4 Hz), and (3) avoid any immediate repetition of individual tones, particularly the tone of interest[57].

These parameters minimize short-term frequency-specific adaptation in the IC while keeping long-term effects to a practical minimum[125], as adaptation in the rat IC can persist even at rates as low as one repetition per second[125,126]. Consequently, DEV-evoked responses may still exhibit marginal frequency-specific adaptation[56], which will similarly affect tones in control sequences when matched for rate and probability. The purpose of these criteria is therefore not to eliminate adaptation entirely, but to ensure that DEV and control responses experience comparable levels of refractoriness, enabling the isolation of higher-order predictive processes.

We chose CAS over the traditional many standards control, which presents the DEV tone among randomly assorted tones. Although the many standards control ensures low repetition, it introduces contextual uncertainty and unpredictable frequency transitions, reducing the likelihood of high-precision predictions[58,127]. CAS addresses these limitations by presenting tones in structured, non-repeating sequences, making it a more effective control for isolating higher-order predictive processing. All stimulus conditions (DEV, CAS, STD) and experimental groups were interleaved across sessions to minimize batch effects and temporal drift. A more

detailed methodology regarding single-unit recordings is found in previous studies[43,59].

Data analysis

All data analysis and data visualization were performed with MATLABR2022b software, using the built-in functions, the Statistics and Machine Learning toolbox, and custom scripts and functions developed in our laboratory. The data and code used in this study are available upon direct request to the corresponding author.

Taking the 40 trials available for each tone within each condition (DEV, STD, and CAS), a peri-stimulus time histogram was computed to represent action potential density from −75 to 250 ms relative to stimulus onset. This histogram was smoothed with a 6 ms Gaussian kernel (MATLAB *ksdensity* function) in 1 ms steps to estimate the spike-density function over time (Fig. 4, Supplementary Data 1). Spike-density functions were expressed as firing rates (spikes/s), reflecting normalization by trial count and kernel width, consistent with previous work[32]. The pre-stimulus baseline firing rate was defined as the average firing rate during the 75 ms preceding stimulus onset.

Evoked excitatory responses were quantified by integrating the area of the spike-density function above the pre-stimulus baseline firing rate between 0 and 180 ms after stimulus onset. Only positive values were retained to avoid negative response estimates. This measure is referred to as the baseline-corrected spike count. Only the last STD tone preceding each DEV tone was included in the analyses.

We only analyzed excitatory responses, since we look primarily for enhancement of responses to deviant tones. To test for the statistical significance of the baseline-corrected spike count, we used a Monte Carlo approach. This method consists of a probability simulation that withdraws numerical values from several random samplings. First, 1000 peristimulus time histograms were simulated using a Poisson model with a constant firing rate equal to the baseline firing rate. With this collection of histograms, we generated a null distribution of baseline-corrected spike counts. Finally, we computed the p value of the original baseline-corrected spike count as $p = (g + 1)/(N + 1)$, where g is the count of null measures greater than or equal to the baseline-corrected spike count, and $N = 1000$ is the size of the null sample. Hence, the Monte Carlo method allowed us to remove any unit-frequency combinations without significant firing activity evoked in response to at least one of the conditions in each experimental set (DEV, CAS or STD).

To compute predictive processing indices, CAS was introduced to control for the repetition effects of the oddball paradigm, allowing a dissociation of frequency-specific adaptation into prediction error and repetition suppression components. To enable comparison across neurons, we normalized the baseline-corrected spike counts evoked by each neuron across the three stimulus conditions (DEV, STD, and CAS) as follows:

$$\text{DEV Normalized} = \frac{\text{DEV}}{N};$$

$$\text{STD Normalized} = \frac{\text{STD}}{\text{N}};$$

$$\text{CAS Normalized} = \frac{\text{CAS}}{\text{N}};$$

where

$$N = \sqrt{\text{DEV}^2 + \text{STD}^2 + \text{CAS}^2}$$

corresponds to the Euclidean norm of the response vector (DEV, STD, CAS), computed independently for each neuron. This normalization yields values bounded between 0 and 1 and has a straightforward geometric interpretation. From these normalized responses, we computed the predictive processing indices iMM, iRS, and iPE as follows:

$$\text{iMM} = \text{DEV}_{Normalized} - \text{STD}_{Normalized};$$

$$\text{iRS} = \text{CAS}_{Normalized} - \text{STD}_{Normalized};$$

$$\text{iPE} = \text{DEV}_{Normalized} - \text{CAS}_{Normalized}.$$

These indices are bounded between −1 and 1. The neuronal mismatch index (iMM) is largely equivalent to the classic Common Stimulus-Specific Adaptation Index[32,122].

Statistics and reproducibility

Statistical analysis was carried out using distribution-free, non-parametric tests implemented in MATLAB (R2022b). These included the Friedman test for baseline-corrected spike counts and normalized responses to DEV, CAS and STD, as well as for the iMM, iRS, and iPE (Supplementary Information, Table 7). Significant values are highlighted in bold. For multiple comparison tests, p values were corrected for false discovery rate 0.1 using the Benjamini–Hochberg method.

To investigate how auditory IC division, sex, and rat model influenced single-neuron activity, we fit generalized linear mixed-effects models separately for pre-stimulus baseline activity, evoked brain responses (DEV, CAS, and STD), and predictive indices (iMM, iRS, and iPE)[128]. We aggregated neural activity at the subject level to ensure that each rat contributed a single, unbiased estimate to the group-level models. Fixed effects included IC division (Lemniscal vs. Non-lemniscal), Sex (Female vs. Male), and Rat model (*Grin2b* + /– vs. VPA). Each model incorporated random intercepts for subject identity and random slopes for IC division to capture both between-subject and within-subject variability.

Including random effects was essential given the considerable inter-individual variability inherent to neurodevelopmental research, particularly in developmental and prenatal exposure models. The random effects accounted for between-subject variability, allowing the fixed effects to estimate population-level predictors accurately.

The intraclass correlation coefficient quantified the proportion of variance attributable to between-subject variability. According to the normed and standardized intraclass correlation coefficient[129], values below 0.40 indicate poor concordance, values between 0.40 and 0.59 are considered fair, values from 0.60 to 0.74 are good, and values of 0.75 or higher represent excellent concordance. Higher intraclass correlation coefficient values indicated that a larger proportion of the total variance was attributable to consistent between-subject differences driven by the experimental variables (sex and rat model across each division of the IC), rather than random or within-subject variability.

The model was fitted using the Laplace approximation and optimized with the 'quasinewton' algorithm to improve convergence under high random-effects correlation. We initially attempted non-parametric bootstrapping to estimate confidence intervals and empirical p values. However, due to the limited subject sample and high model complexity, this approach produced unstable estimates and uniformly conservative outcomes. We therefore relied on profile likelihood confidence intervals, which provided stable, interpretable bounds and are theoretically appropriate for inference in small-sample generalized linear mixed-effects models. This approach allowed us to identify robust fixed effects while preserving subject-level variance structure[31,130].

We reported the covariance parameters of the random effects, including standard deviations and correlations, for each neural response in Supplementary Information, Table 8. All models converged successfully. We observed several extreme intercept–slope correlations for IC division ($|r| \geq 0.96$ in DEV, STD, iMM, and iRS), which are characteristic of well-identified models with small random-slope variances for binary factors. Model diagnostics confirmed excellent model stability, and fixed-effects estimates were robust across specifications. We therefore regarded these

correlations as expected numerical outcomes of the model structure rather than indicators of biological or statistical irregularities.

To further interpret the effects of sex, rat model, and IC division identified by the generalized linear mixed-effects models, we computed estimated marginal means and their model-based pairwise contrasts. These contrasts probed specific group differences across sex, rat model, and IC division while preserving the hierarchical structure of the dataset by accounting for neurons nested within animals.

Then, we used neuron-level data to assess the relationship between short-term adaptation decay and iRS by computing Spearman correlations between iRS and the adaptation exponent derived from a power-law fit to the first 10 STD trials. Neuronal responses were modeled using the function $y(t)=a \cdot t^b + c$, where $y(t)$ represents the neuronal response at time t, a indicates the initial response magnitude, or the first spike strength, b quantifies the rate of adaptation across repeated stimuli (with more negative values indicating faster adaptation), and c represents the steady-state response level[59,120,131].

Model fit quality, assessed by the coefficient of determination (R^2), indicated that the power-law function captured a substantial proportion of response variability. In the lemniscal IC, power-law fits accounted for 23.1% to 36.4% of the variance, with mean R^2 values of 0.364 (Control females), 0.236 (Control males), 0.280 (*Grin2b* + /– females), 0.251 (*Grin2b* + /– males), 0.231 (prenatal VPA females), and 0.239 (prenatal VPA males). In contrast, fits in the non-lemniscal division yielded higher R^2 values overall, ranging from 27.6% to 51.4%, with group means of 0.514 (Control females), 0.318 (Control males), 0.496 (*Grin2b* + /– females), 0.384 (*Grin2b* + /– males), 0.276 (prenatal VPA females), and 0.330 (prenatal VPA males). These values indicate that the power-law function captured short-term adaptation dynamics more reliably in the non-lemniscal auditory midbrain, consistent with its greater sensitivity to contextual modulation.

Histology and neuroanatomical location of recording sites

At the end of each experiment, we marked the recording sites by passing a 5 µA current for 5 s through the recording electrode along the electrode track (Fig. 3B). If still alive after the conclusion of the experimental paradigms, animals were euthanised by injecting a lethal dose of pentobarbital. If still alive, animals were sacrificed by being injected with a lethal dose of pentobarbital. After death was confirmed, they were decapitated. Brains were immediately immersed in a mixture of 4% formaldehyde in 0.1 M PB. After fixation, the neural tissue was cryoprotected in 30% sucrose and sectioned in the coronal plane at 40 µm thickness on a freezing microtome. Slices were stained with 0.1% cresyl violet to facilitate identification of cytoarchitectural boundaries (Fig. 3B). Finally, the recorded neurons were assigned to one of the main subdivisions of the IC using the standard sections from a rat brain atlas as reference, as in our previous studies[32,54–56].

The main dataset comprised 253 auditory neurons recorded from the IC of 43 anesthetized Long–Evans rats. Histological analysis identified 263 neurons in the central nucleus of the IC (lemniscal division). These included 71 neurons from control animals (28 from females, 54 from males), 50 from *Grin2b* + /– animals (33 from females, 17 from males), and 142 from prenatally VPA-induced animals (29 from females, 92 from males).

The remaining 221 neurons were in the cortical regions of the IC (non-lemniscal division). Of these, 152 were from control animals (56 from females, 50 from males), 53 from *Grin2b* + /– animals (31 from females, 22 from males), and 79 from prenatally VPA-exposed animals (44 from females, 18 from males).

Generative AI disclosure statement

Generative AI (ChatGPT 5.0) has been strictly used in order to improve the readability and language of the work in some paragraphs of the current paper. No part of the substantive content, arguments, or conclusions was generated by AI; they are solely the work of the author. The authors reviewed and edited the content as needed and take full responsibility for the content of the published article.

Reporting summary

Further information on research design is available in the Nature Portfolio Reporting Summary linked to this article.

Data availability

Source data can be found in the Supplementary Data files. The datasets generated during this study are available from the corresponding author upon reasonable request.

Code availability

The custom code used for data analysis in this study is available on Zenodo (https://doi.org/10.5281/zenodo.17661741).

Received: 20 August 2025; Accepted: 12 January 2026;
Published online: 30 January 2026

References

1. American Psychiatric Association. Diagnostic and Statistical Manual of Mental Disorders https://doi.org/10.1176/APPI.BOOKS.9780890425787 (2022).
2. Gonçalves, A. M. & Monteiro, P. Autism spectrum disorder and auditory sensory alterations: a systematic review on the integrity of cognitive and neuronal functions related to auditory processing. *J. Neural Transm.* **130**, 325 (2023).
3. O'Connor, K. Auditory processing in autism spectrum disorder: a review. *Neurosci. Biobehav Rev.* **36**, 836–854 (2012).
4. Crane, L., Goddard, L. & Pring, L. Sensory processing in adults with autism spectrum disorders. *Autism* **13**, 215–228 (2009).
5. Heaton, P., Davis, R. E. & Happé, F. G. E. Research note: exceptional absolute pitch perception for spoken words in an able adult with autism. *Neuropsychologia* **46**, 2095–2098 (2008).
6. Marco, E. J., Hinkley, L. B. N., Hill, S. S. & Nagarajan, S. S. Sensory processing in autism: a review of neurophysiologic findings. *Pediatr. Res.* **69**, 48R (2011).
7. Gomot, M., Giard, M.-H., Adrien, J.-L., Barthelemy, C. & Bruneau, N. Hypersensitivity to acoustic change in children with autism: electrophysiological evidence of left frontal cortex dysfunctioning. *Psychophysiology* **39**, 577–584 (2002).
8. Bradshaw, J., Schwichtenberg, A. J. & Iverson, J. M. Capturing the complexity of autism: applying a developmental cascades framework. *Child Dev. Perspect.* **16**, 18 (2022).
9. Rotschafer, S. E. Auditory discrimination in autism spectrum disorder. *Front. Neurosci.* **15**, 651209 (2021).
10. Han, Y. K., Köver, H., Insanally, M. N., Semerdjian, J. H. & Bao, S. Early experience impairs perceptual discrimination. *Nat. Neurosci.* **10**, 1191–1197 (2007).
11. Hu, C., Chen, W., Myers, S. J., Yuan, H. & Traynelis, S. F. Human GRIN2B variants in neurodevelopmental disorders. *J. Pharm. Sci.* **132**, 115–121 (2016).
12. Pan, Y. et al. Association of genetic variants of GRIN2B with autism. *Sci. Rep.* **5**, 1–5 (2015).
13. Yoo, H. J., Cho, I. H., Park, M., Yang, S. Y. & Kim, S. A. Family based association of GRIN2A and GRIN2B with Korean autism spectrum disorders. *Neurosci. Lett.* **512**, 89–93 (2012).
14. Taleb, A. et al. Emerging mechanisms of valproic acid-induced neurotoxic events in autism and its implications for pharmacological treatment. *Biomed. Pharmacother.* **137**, 111322 (2021).
15. Ogawa, T., Kuwagata, M., Hori, Y. & Shioda, S. Valproate-induced developmental neurotoxicity is affected by maternal conditions including shipping stress and environmental change during early pregnancy. *Toxicol. Lett.* **174**, 18–24 (2007).
16. Chomiak, T., Turner, N. & Hu, B. What we have learned about autism spectrum disorder from valproic acid. *Patholog. Res. Int.* **2013**, 712758 (2013).

17. Pugsley, K., Scherer, S. W., Bellgrove, M. A. & Hawi, Z. Environmental exposures associated with elevated risk for autism spectrum disorder may augment the burden of deleterious de novo mutations among probands. *Mol. Psychiatry* **27**, 710–730 (2021).
18. Sandin, S. et al. Examining sex differences in autism heritability. *JAMA Psychiatry* **81**, 673–680 (2024).
19. Werling, D. M. & Geschwind, D. H. Sex differences in autism spectrum disorders. *Curr. Opin. Neurol.* **26**, 146–153 (2013).
20. Schaafsma, S. M. & Pfaff, D. W. Etiologies underlying sex differences in autism spectrum disorders. *Front. Neuroendocrinol.* **35**, 255–271 (2014).
21. Giarelli, E. et al. Sex differences in the evaluation and diagnosis of autism spectrum disorders among children. *Disabil. Health J.* **3**, 107–116 (2010).
22. Napolitano, A. et al. Sex differences in autism spectrum disorder: diagnostic, neurobiological, and behavioral features. *Front. Psychiatry* **13**, 889636 (2022).
23. Bitsika, V., Sharpley, C. F. & Mills, R. Sex differences in sensory features between boys and girls with autism spectrum disorder. *Res. Autism Spectr. Disord.* **51**, 49–55 (2018).
24. Mandy, W. et al. Sex differences in autism spectrum disorder: evidence from a large sample of children and adolescents. *J. Autism Dev. Disord.* **42**, 1304–1313 (2012).
25. Friston, K. A theory of cortical responses. *Philos. Trans. R. Soc. Lond. B Biol. Sci.* **360**, 815–836 (2005).
26. Pellicano, E. & Burr, D. When the world becomes too real: a Bayesian explanation of autistic perception. *Trends Cogn. Sci.* **16**, 504–510 (2012).
27. Sinha, P. et al. Autism as a disorder of prediction. *Proc. Natl. Acad. Sci. USA* **111**, 15220–15225 (2014).
28. van Boxtel, J. J. A. & Lu, H. A predictive coding perspective on autism spectrum disorders. *Front. Psychol.* **4**, 40641 (2013).
29. van de Cruys, S. et al. Precise minds in uncertain worlds: predictive coding in autism. *Psychol. Rev.* **121**, 649–675 (2014).
30. Rapaport, H. & Sowman, P. F. Examining predictive coding accounts of typical and autistic neurocognitive development. *Neurosci. Biobehav Rev.* **167**, 105905 (2024).
31. Parras, G. G., Valdés-Baizabal, C., Harms, L., Michie, P. T. & Malmierca, M. S. The effect of NMDA-R antagonist, MK-801, on neuronal mismatch along the rat auditory thalamocortical pathway. *Sci. Rep.* **10**, 1–19 (2020).
32. Parras, G. G. et al. Neurons along the auditory pathway exhibit a hierarchical organization of prediction error. *Nat. Commun.* **8**, 1–17 (2017).
33. D'Mello, A. M. et al. Diminished repetition suppression reveals selective and systems-level face processing differences in ASD. *J. Neurosci.* **43**, 1952–1962 (2023).
34. Ewbank, M. P. et al. Repetition suppression and memory for faces is reduced in adults with autism spectrum conditions. *Cereb. Cortex* **27**, 92–103 (2017).
35. Ewbank, M. P. et al. Repetition suppression in ventral visual cortex is diminished as a function of increasing autistic traits. *Cereb. Cortex* **25**, 3381–3393 (2015).
36. Lacroix, A. et al. Sex modulation of faces prediction error in the autistic brain. *Commun. Biol.* **7**, 1–12 (2024).
37. Dunn, M. A., Gomes, H. & Gravel, J. Mismatch negativity in children with autism and typical development. *J. Autism Dev. Disord.* **38**, 52–71 (2008).
38. Vlaskamp, C. et al. Auditory processing in autism spectrum disorder: mismatch negativity deficits. *Autism Res.* **10**, 1857–1865 (2017).
39. Chen, T. C., Hsieh, M. H., Lin, Y. T., Chan, P. Y. S. & Cheng, C. H. Mismatch negativity to different deviant changes in autism spectrum disorders: a meta-analysis. *Clin. Neurophysiol.* **131**, 766–777 (2020).
40. Schwartz, S., Shinn-Cunningham, B. & Tager-Flusberg, H. Meta-analysis and systematic review of the literature characterizing auditory mismatch negativity in individuals with autism. *Neurosci. Biobehav Rev.* **87**, 106–117 (2018).
41. Lassen, J. et al. Reduced mismatch negativity in children and adolescents with autism spectrum disorder is associated with their impaired adaptive functioning. *Autism Res.* **15**, 1469–1481 (2022).
42. da Silva Mayerle, M. C. C., Riesgo, R., Gregory, L., Borges, V. M. S. & Sleifer, P. Mismatch negativity in children and adolescents with autism spectrum disorder. *Int Arch. Otorhinolaryngol.* **27**, e218 (2023).
43. Carbajal, G. V., Casado-Román, L. & Malmierca, M. S. Two prediction error systems in the nonlemniscal inferior colliculus: 'spectral' and 'nonspectral'. *J. Neurosci.* **44**, e1293232023 (2024).
44. Malmierca. Chapter 29 – auditory system. *The rat nervous system (Paxinos G, ed.)* 865–946 https://www.sciencedirect.com/book/9780123742452/the-rat-nervous-system (2015).
45. Macias, S. & Llano, D. A. Descending projections to the auditory midbrain: evolutionary considerations. *J. Comp. Physiol.* **209**, 131–143 (2023).
46. Frisina, R. D. Subcortical neural coding mechanisms for auditory temporal processing. *Hear Res.* **158**, 1–27 (2001).
47. Frisina, R. D., Walton, J. P., Lynch-Armour, M. A. & Byrd, J. D. Inputs to a physiologically characterized region of the inferior colliculus of the young adult CBA mouse. *Hear Res.* **115**, 61–81 (1998).
48. Ingham, N. J. & McAlpine, D. GABAergic inhibition controls neural gain in inferior colliculus neurons sensitive to interaural time differences. *J. Neurosci.* **25**, 6187–6198 (2005).
49. Ingham, N. J. & McAlpine, D. Spike-frequency adaptation in the inferior colliculus. *J. Neurophysiol.* **91**, 632–645 (2004).
50. Duque, D. & Malmierca, M. S. Stimulus-specific adaptation in the inferior colliculus of the mouse: anesthesia and spontaneous activity effects. *Brain Struct. Funct.* **220**, 3385–3398 (2015).
51. Malmierca, M. S. et al. Pattern-sensitive neurons reveal encoding of complex auditory regularities in the rat inferior colliculus. *Neuroimage* **184**, 889–900 (2019).
52. Valdés-Baizabal, C., Casado-Román, L., Bartlett, E. L. & Malmierca, M. S. In vivo whole-cell recordings of stimulus-specific adaptation in the inferior colliculus. *Hear Res.* **399**, 107978 (2021).
53. Duque, D., Pérez-González, D., Ayala, Y. A., Palmer, A. R. & Malmierca, M. S. Topographic distribution, frequency, and intensity dependence of stimulus-specific adaptation in the inferior colliculus of the rat. *J. Neurosci.* **32**, 17762 (2012).
54. Duque, D., Wang, X., Nieto-Diego, J., Krumbholz, K. & Malmierca, M. S. Neurons in the inferior colliculus of the rat show stimulus-specific adaptation for frequency, but not for intensity. *Sci. Rep.* **6**, 1–15 (2016).
55. Ayala, Y. A., Pérez-González, D., Duque, D., Nelken, I. & Malmierca, M. S. Frequency discrimination and stimulus deviance in the inferior colliculus and cochlear nucleus. *Front. Neural Circuits* **6**, 95 (2013).
56. Malmierca, M. S., Cristaudo, S., Pérez-González, D. & Covey, E. Stimulus-specific adaptation in the inferior colliculus of the anesthetized rat. *J. Neurosci.* **29**, 5483–5493 (2009).
57. Malmierca, M. S. & Casado-Román, L. Novelty processing in the auditory system: detection, adaptation or expectation? in *The Senses: A Comprehensive Reference* Vol. 2 (eds. Fritzsch, B. & Grothe, B.) 749–776 (Elsevier, 2020).
58. Cacciato-Salcedo, S., Lao-Rodríguez, A. B. & Malmierca, M. S. Contextual auditory processing in the inferior colliculus is affected in a sex- and age-dependent manner in the valproic acid-induced rat model of autism. *PLoS Biol.* **23**, e3003309 (2025).
59. Yu, Z. et al. Beyond t-test and ANOVA: applications of mixed-effects models for more rigorous statistical analysis in neuroscience research. *Neuron* **110**, 21–35 (2022).
60. Brehm, L. & Alday, P. M. Contrast coding choices in a decade of mixed models. *J. Mem. Lang.* **125**, 104334 (2022).

61. Ruytjens, L. et al. Functional sex differences in human primary auditory cortex. *Eur. J. Nucl. Med. Mol. Imaging* **34**, 2073 (2007).
62. Krizman, J., Skoe, E. & Kraus, N. Sex differences in auditory subcortical function. https://doi.org/10.1016/j.clinph.2011.07.037 (2011).
63. Esposito, G., Van Horn, J. D., Weinberger, D. R. & Berman, K. F. Gender differences in cerebral blood flow as a function of cognitive state with PET. *J. Nucl. Med.* **37**, 559–564 (1996).
64. Ragland, J. D., Coleman, A. R., Gur, R. C., Glahn, D. C. & Gur, R. E. Sex differences in brain-behavior relationships between verbal episodic memory and resting regional cerebral blood flow. *Neuropsychologia* **38**, 451–461 (2000).
65. Gibson, J. R., Bartley, A. F., Hays, S. A. & Huber, K. M. Imbalance of neocortical excitation and inhibition and altered UP states reflect network hyperexcitability in the mouse model of fragile X syndrome. *J. Neurophysiol.* **100**, 2615–2626 (2008).
66. Lazaro, M. T. et al. Reduced prefrontal synaptic connectivity and disturbed oscillatory population dynamics in the CNTNAP2 model of autism. *Cell Rep.* **27**, 2567 (2019).
67. Peñagarikano, O. et al. Absence of CNTNAP2 leads to epilepsy, neuronal migration abnormalities, and core autism-related deficits. *Cell* **147**, 235–246 (2011).
68. Peixoto, R. T., Wang, W., Croney, D. M., Kozorovitskiy, Y. & Sabatini, B. L. Early hyperactivity and precocious maturation of corticostriatal circuits in Shank3B(-/-) mice. *Nat. Neurosci.* **19**, 716–724 (2016).
69. Hull, J. V. et al. Resting-state functional connectivity in autism spectrum disorders: a review. *Front. Psychiatry* **7**, 205 (2017).
70. Zhu, C., Ma, X., Ji, L., Chen, S. & Cao, X. Sex differences in categorical adaptation for faces and chinese characters during early perceptual processing. *Front. Hum. Neurosci.* **11**, 298996 (2018).
71. Nagy, E., Potts, G. F. & Loveland, K. A. Sex-related ERP differences in deviance detection. *Int. J. Psychophysiol.* **48**, 285–292 (2003).
72. Rippon, G. Differently different?: A commentary on the emerging social cognitive neuroscience of female autism. *Biol. Sex. Differ.* **15**, 1–16 (2024).
73. Hull, L., Petrides, K. V. & Mandy, W. The female autism phenotype and camouflaging: a narrative review. *Rev. J. Autism Dev. Disord.* **7**, 306–317 (2020).
74. Baron-Cohen, S. imon S. Empathizing, systemizing, and the extreme male brain theory of autism. *Prog. Brain Res.* **186**, 167–175 (2010).
75. Møller, A. R., Kern, J. K. & Grannemann, B. Are the non-classical auditory pathways involved in autism and PDD? *Neurol. Res.* **27**, 625–629 (2005).
76. Lee, C. C. Exploring functions for the non-lemniscal auditory thalamus. *Front. Neural Circuits* **9**, 69 (2015).
77. Bartlett, E. L., Stark, J. M., Guillery, R. W. & Smith, P. H. Comparison of the fine structure of cortical and collicular terminals in the rat medial geniculate body. *Neuroscience* **100**, 811–828 (2000).
78. Lee, C. C. & Murray Sherman, S. Topography and physiology of ascending streams in the auditory tectothalamic pathway. *Proc. Natl. Acad. Sci. USA* **107**, 372–377 (2010).
79. Ibrahim, B. A. et al. Developmental exposure to polychlorinated biphenyls prevents recovery from noise-induced hearing loss and disrupts the functional organization of the inferior colliculus. *J. Neurosci.* **43**, 4580 (2023).
80. Moller, A. R. & Rollins, P. R. The non-classical auditory pathways are involved in hearing in children but not in adults. *Neurosci. Lett.* **319**, 41–44 (2002).
81. Lukose, R., Schmidt, E., Wolski, T. P., Murawski, N. J. & Kulesza, R. J. Malformation of the superior olivary complex in an animal model of autism. *Brain Res.* **1398**, 102–112 (2011).
82. Zimmerman, R., Patel, R., Smith, A., Pasos, J. & Kulesza, R. J. Repeated prenatal exposure to valproic acid results in auditory brainstem hypoplasia and reduced calcium binding protein immunolabeling. *Neuroscience* **377**, 53–68 (2018).
83. Mabunga, D. F. N., Gonzales, E. L. T., Kim, J., Kim, K. C. & Shin, C. Y. Exploring the validity of valproic acid animal model of autism. *Exp. Neurobiol.* **24**, 285–300 (2015).
84. Gzielo, K. et al. Valproic acid exposure impairs ultrasonic communication in infant, adolescent and adult rats. *Eur. Neuropsychopharmacol.* **41**, 52–62 (2020).
85. Potasiewicz, A., Gzielo, K., Popik, P. & Nikiforuk, A. Effects of prenatal exposure to valproic acid or poly(I:C) on ultrasonic vocalizations in rat pups: the role of social cues. *Physiol. Behav.* **225**, 113110 (2020).
86. Mansour, Y., Mangold, S., Chosky, D. & Kulesza, R. J. Auditory midbrain hypoplasia and dysmorphology after prenatal valproic acid exposure. *Neuroscience* **396**, 79–93 (2019).
87. Mansour, Y. & Kulesza, R. Three dimensional reconstructions of the superior olivary complex from children with autism spectrum disorder. *Hear Res.* **393**, 107974 (2020).
88. Mansour, Y., Ahmed, S. N. & Kulesza, R. Abnormal morphology and subcortical projections to the medial geniculate in an animal model of autism. *Exp. Brain Res.* **239**, 381–400 (2021).
89. Malhotra, A. S. & Kulesza, R. Abnormal auditory brainstem responses in an animal model of autism spectrum disorder. *Hear Res.* **436**, 108816 (2023).
90. Kosmer, K. & Kulesza, R. Cortical dysmorphology and reduced cortico-collicular projections in an animal model of autism spectrum disorder. *Cereb. Cortex* **34**, 146–160 (2024).
91. Kutsuwada, T. et al. Impairment of suckling response, trigeminal neuronal pattern formation, and hippocampal LTD in NMDA receptor ε2 subunit mutant mice. *Neuron* **16**, 333–344 (1996).
92. Watanabe, M., Inoue, Y., Sakimura, K. & Mishina, M. Developmental changes in distribution of NMDA receptor channel subunit mRNAs. *Neuroreport* **3**, 1138–1140 (1992).
93. MISHINA, M. et al. Molecular and functional diversity of the NMDA receptor channel. *Ann. N. Y Acad. Sci.* **707**, 136–152 (1993).
94. Brigman, J. L. et al. GluN2B in corticostriatal circuits governs choice learning and choice shifting. *Nat. Neurosci.* **16**, 1101–1110 (2013).
95. Brigman, J. L. et al. Loss of GluN2B-containing NMDA receptors in CA1 hippocampus and cortex impairs long-term depression, reduces dendritic spine density, and disrupts learning. *J. Neurosci.* **30**, 4590–4600 (2010).
96. Tang, Y. P. et al. Genetic enhancement of learning and memory in mice. *Nature* **401**, 63–69 6748 401 (1999).
97. Shin, W. et al. Early correction of synaptic long-term depression improves abnormal anxiety-like behavior in adult GluN2B-C456Y-mutant mice. *PLoS Biol.* **18**, e3000717 (2020).
98. Wang, X. et al. Potentiation of glutamatergic synaptic transmission onto dorsal raphe serotonergic neurons in the valproic acid model of autism. *Front. Pharmacol.* **9**, 988 (2018).
99. Rinaldi, T., Silberberg, G. & Markram, H. Hyperconnectivity of local neocortical microcircuitry induced by prenatal exposure to valproic acid. *Cereb. Cortex* **18**, 763–770 (2008).
100. Lin, H. C., Gean, P. W., Wang, C. C., Chan, Y. H. & Chen, P. S. The amygdala excitatory/inhibitory balance in a valproate-induced rat autism model. *PLoS One* **8**, e55248 (2013).
101. Wang, C. C. et al. Valproic acid mediates the synaptic excitatory/inhibitory balance through astrocytes - a preliminary study. *Prog. Neuropsychopharmacol. Biol. Psychiatry* **37**, 111–120 (2012).
102. Durieux, A. M. S., Horder, J. & Petrinovic, M. M. Neuroligin-2 and the tightrope of excitation/inhibition balance in the prefrontal cortex. *J. Neurophysiol.* **115**, 5–7 (2016).
103. Gonzalez-Gadea, M. L. et al. Predictive coding in autism spectrum disorder and attention deficit hyperactivity disorder. *J. Neurophysiol.* **114**, 2625 (2015).
104. Bosch, E., Fritsche, M., Utzerath, C., Buitelaar, J. K. & de Lange, F. P. Adaptation and serial choice bias for low-level visual features are unaltered in autistic adolescents. *J. Vis.* **22**, 1–1 (2022).

105. Nourski, K. V. et al. Auditory predictive coding across awareness states under anesthesia: an intracranial electrophysiology study. *J. Neurosci.* **38**, 8441–8452 (2018).
106. Nourski, K. V. et al. Cortical responses to auditory novelty across task conditions: an intracranial electrophysiology study. *Hear. Res.* **399**, 107938 (2021).
107. Petrinovic, M. M. et al. A novel anesthesia regime enables neurofunctional studies and imaging genetics across mouse strains. *Sci. Rep.* **6**, 1–12 (2016).
108. Hara, K. & Harris, R. A. The anesthetic mechanism of urethane: the effects on neurotransmitter-gated ion channels. *Anesth. Analg.* **94**, 313–318 (2002).
109. Maggi, C. A. & Meli, A. Suitability of urethane anesthesia for physiopharmacological investigations in various systems. Part 1: General considerations. *Experientia* **42**, 109–114 (1986).
110. Sengupta, P. The laboratory rat: relating its age with human's. *Int. J. Prev. Med* **4**, 624 (2013).
111. Nicolini, C. & Fahnestock, M. The valproic acid-induced rodent model of autism. *Exp. Neurol.* **299**, 217–227 (2018).
112. Chaliha, D. et al. A systematic review of the valproic-acid-induced rodent model of autism. *Dev. Neurosci.* **42**, 12–48 (2020).
113. Gogolla, N. et al. Common circuit defect of excitatory-inhibitory balance in mouse models of autism. *J. Neurodev. Disord.* **1**, 172–181 (2009).
114. Ehlers, K., Stürje, H., Merker, H. & Nau, J. H. Valproic acid-induced spina bifida: a mouse model. *Teratology* **45**, 145–154 (1992).
115. Kim, K. C. et al. The critical period of valproate exposure to induce autistic symptoms in Sprague-Dawley rats. *Toxicol. Lett.* **201**, 137–142 (2011).
116. Favre, M. R. et al. General developmental health in the VPA-rat model of autism. *Front. Behav. Neurosci.* **7**, 88 (2013).
117. Sceniak, M. P. & MacIver, M. B. Cellular actions of urethane on rat visual cortical neurons in vitro. *J. Neurophysiol.* **95**, 3865–3874 (2006).
118. Nieto-Diego, J. & Malmierca, M. S. Topographic distribution of stimulus-specific adaptation across auditory cortical fields in the anesthetized rat. *PLoS Biol.* **14**, e1002397 (2016).
119. Näätänen, R., Astikainen, P., Ruusuvirta, T. & Huotilainen, M. Automatic auditory intelligence: an expression of the sensory-cognitive core of cognitive processes. *Brain Res Rev.* **64**, 123–136 (2010).
120. Ulanovsky, N., Las, L. & Nelken, I. Processing of low-probability sounds by cortical neurons. *Nat. Neurosci.* **6**, 391–398 (2003).
121. Carbajal, G. V. & Malmierca, M. S. The neuronal basis of predictive coding along the auditory pathway: from the subcortical roots to cortical deviance detection. *Trends Hear.* **22**, 2331216518784822 (2018).
122. Todorovic, A. & de Lange, F. P. Repetition suppression and expectation suppression are dissociable in time in early auditory evoked fields. *J. Neurosci.* **32**, 13389–13395 (2012).
123. Ruhnau, P., Herrmann, B. & Schröger, E. Finding the right control: the mismatch negativity under investigation. *Clin. Neurophysiol.* **123**, 507–512 (2012).
124. Zhao, L., Liu, Y., Shen, L., Feng, L. & Hong, B. Stimulus-specific adaptation and its dynamics in the inferior colliculus of rat. *Neuroscience* **181**, 163–174 (2011).
125. Pérez-González, D., Malmierca, M. S. & Covey, E. Novelty detector neurons in the mammalian auditory midbrain. *Eur. J. Neurosci.* **22**, 2879–2885 (2005).
126. Harms, L. et al. Mismatch negativity (MMN) in freely-moving rats with several experimental controls. *PLoS One* **9**, e110892 (2014).
127. McCulloch, C. E., Searle, S. R. & Neuhaus, J. M. *Generalized, Linear, and Mixed Models* 2nd edn, 424 (Wiley, 2008).
128. Cicchetti, D. V. Guidelines, criteria, and rules of thumb for evaluating normed and standardized assessment instruments in psychology. *Psychol. Assess.* **6**, 284–290 (1994).
129. Bates, D., Mächler, M., Bolker, B. M. & Walker, S. C. Fitting linear mixed-effects models using lme4. *J. Stat. Softw.* **67**, 1–48 (2015).
130. Stroup, W. W., Ptukhina, M. & Garai, J. Generalized linear mixed models: modern concepts, methods and applications. *Nat. Res.* **1**, 668 (2024).
131. Valdés-Baizabal, C., Carbajal, G. V., Pérez-González, D. & Malmierca, M. S. Dopamine modulates subcortical responses to surprising sounds. *PLoS Biol.* **18**, e3000744 (2020).

Acknowledgements

This study was supported by projects PID2023-148541OB-I00, funded by MICIU/AEI /10.13039/501100011033; the Consejería de Educación, Junta de Castilla y León (SA218P23), and the strategic research programs of excellence from the Regional Government of Castile and León, co-funded by the ERDF Operational Program (ref. CLU-2023-1-01), awarded to M.S.M.; and a fellowship from the Spanish Ministry of Science and Universities (FPU2021/00124) to S.C.S. The funders had no role in study design, data collection and analysis, decision to publish, or preparation of the manuscript.

Author contributions

S.C.S.: conceptualization, methodology, formal analysis, investigation, visualization; data curation; writing—original draft, writing—review & editing. A.B.L.R.: investigation, methodology, writing—review & editing. M.S.M.: conceptualization, writing - original draft; writing—review & editing, supervision, funding acquisition and project administration.

Competing interests

The authors declare no competing interests.

Additional information

Supplementary information The online version contains supplementary material available at https://doi.org/10.1038/s42003-026-09585-z.

Correspondence and requests for materials should be addressed to Manuel S. Malmierca.

Peer review information *Communications Biology* thanks the anonymous reviewers for their contribution to the peer review of this work. Primary Handling Editors: Zenas Chao and Jasmine Pan. A peer review file is available.